J Comput Neurosci
DOI 10.1007/s10827-008-0117-3

Synchronization properties of networks of electrically coupled neurons in the presence of noise and heterogeneities

Srdjan Ostojic · Nicolas Brunel · Vincent Hakim

Received: 22 June 2008 / Revised: 1 October 2008 / Accepted: 3 October 2008

Abstract We investigate how synchrony can be generated or induced in networks of electrically coupled integrate-and-fire neurons subject to noisy and heterogeneous inputs. Using analytical tools, we find that in a network under constant external inputs, synchrony can appear via a Hopf bifurcation from the asynchronous state to an oscillatory state. In a homogeneous network, in the oscillatory state all neurons fire in synchrony, while in a heterogeneous network synchrony is looser, many neurons skipping cycles of the oscillation. If the transmission of action potentials via the electrical synapses is effectively excitatory, the Hopf bifurcation is supercritical, while effectively inhibitory transmission due to pronounced hyperpolarization leads to a subcritical bifurcation. In the latter case, the network exhibits bistability between an asynchronous state and an oscillatory state where all the neurons fire in synchrony. Finally we show that for time-varying external inputs, electrical coupling enhances the synchronization in an asynchronous network via a resonance at the firing-rate frequency.

Action Editor: Alain Destexhe

S. Ostojic (✉) · V. Hakim
Laboratoire de Physique Statistique,
CNRS UMR 8550, Ecole Normale Supérieure,
75231 Paris Cedex 05, France
e-mail: srdjan@lps.ens.fr

N. Brunel
Laboratory of Neurophysics and Physiology,
CNRS UMR 8119, Université Paris Descartes,
Paris, France

Keywords Gap junctions · Oscillations · Neural networks

1 Introduction

A number of experimental studies have revealed the presence of electrical coupling via gap junctions in the mammalian brain (Galarreta and Hestrin 1999, 2001a, b, 2002; Gibson et al. 1999; Mann-Metzer and Yarom 1999; Beierlein et al. 2000; Landisman et al. 2002; Bennett and Zukin 2004; Connors and Long 2004; Galarreta et al. 2004; Hestrin and Galarreta 2005). While electrical synapses have long been known to play a role in the nervous systems of invertebrates as well as in development, electrophysiological recordings in pairs of neurons have now also unambiguously identified them in various areas of the adult mammalian central nervous system, in particular in the neocortex (Galarreta and Hestrin 1999; Gibson et al. 1999; Beierlein et al. 2000), thalamus (Landisman et al. 2002), hippocampus (Draguhn et al. 1998; Fukuda and Kosaka 2000; Venance et al. 2000; LeBeau et al. 2003) and cerebellum (Mann-Metzer and Yarom 1999; Dugué et al. 2008). As they have been found predominantly between GABAergic cells of a same class, it has been proposed that electrical synapses define local, highly-connected network modules. The function of these modules has so far remained unclear, but it has been proposed that they might contribute to the generation of network rhythms, or act as coincidence detectors (Galarreta et al. 2004; Hestrin and Galarreta 2005). Indeed, in many cases, electrical interactions via gap junctions have been related to observed synchrony in

the dynamics of the underlying network (Draguhn et al. 1998; Skinner et al. 1999; Mann-Metzer and Yarom 1999; Tamas et al. 2000; Traub et al. 2001). It is thus important to understand on a mechanistic level whether and how electrical synapses affect synchrony in a network of neurons.

Intuitively, it seems clear that gap junctions, which in the first approximation can be seen as simple ohmic conductances, tend to equalize membrane potentials of the neurons they connect, and thus contribute to synchronizing their activity, at least while the membrane potential remains subthreshold. However, once a neuron spikes, the effect of gap junctions can be more subtle as the post-synaptic neurons receive a low-pass filtered version of the action potential called a "spikelet" (Galarreta and Hestrin 2001a). Due to filtering, the fast, depolarizing part of the spike is transmitted less than the slower, hyper-polarizing part, and the net effect of spike transmission can be either excitatory or inhibitory depending on the overall shape of a pre-synaptic action potential. The effect of gap junctions on synchrony is thus far from obvious and needs careful investigation.

While a large number of theoretical investigations have been devoted to the effects of chemical synapses on synchrony, electrical synapses have received less attention (Sherman and Rinzel 1992; Chow and Kopell 2000; Lewis and Rinzel 2003; Pfeuty et al. 2003, 2005; Kopell and Ermentrout 2004; Bem et al. 2005; Schneider et al. 2006; Coombes and Zachariou 2008; Coombes 2008). In particular, these studies mostly considered homogeneous networks in the low-noise regime, where all neurons fire in a regular fashion at an identical firing rate. The main conclusion is that, in contrast to common intuition, electrical coupling can provide either synchrony or asynchrony, depending on the firing frequency and the shape of the action potentials.

In physiological conditions, due to the large number of synaptic connections, neurons receive a noisy input, and therefore fire in an irregular manner. Moreover, different neurons vary in excitability, and typically receive a different mean input, which results in a large distribution of mean firing rates over the network. Clearly, synchrony is much more difficult to achieve in these conditions. Nevertheless, in a recent study of the Golgi cell cerebellar network (Dugué et al. 2008) it has been shown experimentally and numerically that electrical coupling can lead to synchrony in noisy and heterogeneous networks. It has also been shown in this study that electrical coupling can resonantly enhance the network response to oscillatory inputs at a preferred frequency. The aim of the present work is to provide an analytical understanding of the effects of electrical coupling on synchronization in presence of noise and heterogeneities. To this end, we consider a network of electrically coupled, leaky integrate-and-fire neurons and examine its dynamics by extending the analytical approach developed for networks of chemically coupled neurons (Brunel and Hakim 1999; Brunel 2000).

In a first part, we study the nature of the dynamics in networks where neurons receive noisy currents of constant mean and standard deviation (noise intensity). We start with homogeneous networks where the mean current and the noise intensity are identical for all neurons, and then turn to the heterogeneous case. In both situations, at large noise intensities, the network is found to be in an asynchronous state. As noise is reduced, this state loses stability via a Hopf bifurcation, and an oscillatory stable state emerges. We determine this stability boundary analytically for different input and coupling parameters. Combining a weakly nonlinear analysis with direct numerical simulations, we find that if the spike transmission via the gap junctions is dominantly inhibitory, the bifurcation is subcritical, and the dynamics are bistable: in a large region of parameter space, depending on its history the network can be found either in the asynchronous state or in a fully synchronous state. In the heterogeneous case, the dynamics display the same features, although both the synchronous state and the bistable region are less resistant to noise.

In a second part of this article, we examine how time-dependent inputs can induce oscillations in an electrically coupled network originally in an asynchronous state. We determine the response of the network to sinusoidally modulated currents of different frequencies, and show that the coupling between the neurons leads to large resonances corresponding to the synchronization of firing between neurons. We also show that in the bistable region, strong synchronous inputs can switch the network activity between synchrony and asynchrony.

The outline of the article is as follows. In Section 2 we present in detail our model, a network of electrically coupled, leaky integrate-and-fire neurons, as well as the parameters which we study. In Section 3, we analyze the dynamics of a homogeneous network, and determine phase diagrams showing the nature of its dynamics (asynchronous or oscillatory) in different regions of parameter space. In Section 4, we extend these results to heterogeneous networks. In Section 5, we examine the induction of oscillations by time-dependent inputs.

Finally in Section 6, we discuss the consequence of our findings, and their relationship with results of previous studies.

2 Integrate-and-fire model of electrically coupled neurons

The model we study is a network of N single-compartment leaky integrate-and-fire (LIF) neurons. The dynamics of the membrane potential V_i of neuron i ($i = 1, \ldots, N$) is given by

$$c_m \frac{dV_i}{dt} = -g_m V_i + I_i^{int} + I_i^{ext} \tag{1}$$

Here c_m and g_m are the membrane capacitance and conductance, I_i^{int} is the current due to the interactions with other cells within the network, and I_i^{ext} is an external input current flowing into each cell. When V_i reaches a threshold value V_{th}, the cell fires an action potential and V_i is reset to a value V_r.

The external current I_i^{ext} represents the collective effect of inputs coming from other areas, outside of the studied network. It is modeled as

$$I_i^{ext} = I_i^{ext}(t) + \Delta \eta_i(t) \tag{2}$$

where I_i^{ext} is the (possibly time-dependent) mean value of the input, Δ measures the amplitude of input fluctuations and η_i is a gaussian white noise term independent from neuron to neuron, $\langle \eta_i(t) \rangle = 0$ and $\langle \eta_i(t) \eta_j(t') \rangle = \delta_{ij} \delta(t - t')$.

The interaction current I_i^{int} represents the effect of gap junctions connecting neuron i and other neurons within the network. Electrical coupling via gap junctions between neurons i and j is usually modeled as a simple ohmic conductance between their membranes, $I_{ij}^{gap} = \gamma_{gap}(V_j - V_i)$. In the case of LIF neurons, the membrane potential is known only in the subthreshold domain, as the precise voltage trace of the spike is ignored. To take into account the effect of spike transmission through gap junctions, we follow the approach of Lewis and Rinzel (2003): when neuron j spikes, the transmission of the fast, depolarizing part of the action potential is effectively represented as an instantaneous excitatory pulse delivered to all other neurons connected to it. The strength of this pulse is measured by a parameter β_{gap}. The full amplitude of the pulse, which we take to be $\beta_{gap} c_m$ (the factor c_m is introduced to have β_{gap} in units of mV), corresponds to the amount of charge transferred during the depolarizing part of the spike.[1] The total coupling current I_{ij}^{int} received by cell i from cell j is thus

$$I_{ij}^{int} = \gamma_{gap}(V_j - V_i) + \beta_{gap} c_m \sum_{n_j=-\infty}^{0} \delta(t - t_{n,j}) \tag{3}$$

where $t_{n,j}$ is the time of the n^{th} spike of cell j.

When the neuron j emits an action potential, a neuron i connected to it first receives a depolarizing pulse, and then a hyperpolarizing current due to the reset of neuron j, mediated by the subthreshold electrical coupling. Figure 1 illustrates the shapes of the post-synaptic spikelets in the model, for two different sets of parameters corresponding respectively to a predominantly excitatory and inhibitory effect of the spike transmission through the electrical synapse. It should be noted that the precise shape and size of the spikelet depends of course on the voltage in the post-synaptic cell at the time the action potential is emitted. The relationship between the parameter β_{gap} and the actual shape of the action potential is explored in more detail in Appendix A, where we consider full traces of action potentials obtained from the exponential integrate and fire model (Fourcaud-Trocmé et al. 2003).

We study a fully connected network in which every neuron is coupled to all others via Eq. (3). The coupling strengths are taken to scale inversely with the size of the

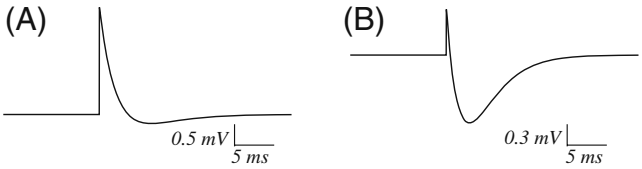

Fig. 1 Spikelets in a post-synaptic cell elicited by the transmission of a pre-synaptic spike through an electrical synapse, obtained from the leaky integrate-and-fire model for two different sets of coupling parameters. (**A**) Dominantly excitatory spikelet $\gamma_{gap} = 0.26$, $\beta_{gap} = 5$ mV; (**B**) dominantly inhibitory spikelet $\gamma_{gap} = 0.33$, $\beta_{gap} = 2$ mV. In both cases, both cells are initially at their resting potential (0 mV). A very brief transient current is injected in the pre-synaptic cell, leading this cell to spike, and evoking the shown post-synapting spikelet in the post-synaptic cell. $V_r = -10$ mV and $V_{th} = 20$ mV

[1] Clearly, the amount of charge transferred during any portion of the spike is proportional to γ_{gap}. Here we deliberately treat β_{gap} and γ_{gap} as independent parameters to be able to consider the case $\gamma_{gap} = 0$ while $\beta_{gap} \neq 0$.

network, $\gamma_{gap} = \gamma_c/N$ and $\beta_{gap} = \beta/N$. The evolution equation Eq. (1) then reads

$$c_m \frac{dV_i}{dt} = -g_m V_i + \frac{\gamma_c}{N}\sum_{j\neq i}(V_j - V_i) + \frac{\beta c_m}{N}\sum_j \sum_{n_j=-\infty}^{0} \delta(t - t_{n,j}) + I_i^{ext}(t) + \Delta\eta_i(t) \tag{4}$$

To simplify the notations, it is convenient to introduce the rescaled parameters $\tau = c_m/(g_m + \gamma_c)$, $g_c = \gamma_c/(g_m + \gamma_c)$, $\mu_{ext,i} = I_i^{ext}/(g_m + \gamma_c)$, $\sigma = \Delta/\sqrt{c_m(g_m + \gamma_c)}$. In the following we will work exclusively with the newly defined parameters, but the results can be expressed in terms of old variables using

$$\gamma_c = \frac{g_m g_c}{1 - g_c} \tag{5}$$

$$I_i^{ext} = \frac{g_m}{1 - g_c}\mu_{ext,i} \tag{6}$$

$$\Delta = \frac{\sqrt{g_m c_m}}{1 - g_c}\sigma \tag{7}$$

In terms of the new variables $g_c, \mu_{ext,i}$ and σ the dynamics of the system become

$$\tau \frac{dV_i}{dt} = -V_i + \frac{g_c}{N}\sum_{j\neq i} V_j + \frac{\beta\tau}{N}\sum_j \sum_{n_j=-\infty}^{\infty} \delta(t - t_{n_j}) + \mu_{ext,i}(t) + \sigma\sqrt{\tau}\eta_i(t) \tag{8}$$

Here g_c is the rescaled strength of electrical coupling ($0 \leq g_c \leq 1$), β (in mV) represents the strength of the supra-threshold portion of the spike, μ_{ext} and σ (in mV) correspond to the mean and variance of the external input current. We study the influence of these four parameters μ_{ext}, σ, g_c and β on the dynamics of the network. We keep fixed $\tau_m = c_m/g_m = 20$ ms, $V_r = 10$ mV and $V_{th} = 20$ mV, but if needed their effect can be easily deduced from our analysis. Note that since τ_m is fixed, the value of $\tau = \tau_m(1 - g_c)$ changes when g_c is varied.

3 Analysis of network dynamics: homogeneous case

We first consider a homogeneous network in which all neurons receive a statistically identical, time-independent input current, ie. $\mu_{ext,i}(t) = \mu_{ext}$ and $\sigma_i = \sigma$ for all i. To study analytically the dynamics of the network, we follow the mean-field approach developed in Abbott and van Vreeswijk (1993), Brunel and Hakim (1999), Brunel (2000). Defining the average membrane potential over the population

$$\langle V\rangle(t) = \frac{1}{N}\sum_{j=}^{N} V_j, \tag{9}$$

for large N we write

$$\frac{1}{N}\sum_{j\neq i} V_j(t) \approx \langle V\rangle(t). \tag{10}$$

Moreover, as all neurons are statistically equivalent, they all fire with the same (possibly time-dependent) instantaneous rate $\nu(t)$, so that the term $\frac{1}{N}\sum_j \sum_{n_j=-\infty}^{\infty} \delta(t - t_{n_j})$ in Eq. (8) can be approximated by $\nu(t)$ up to corrections of order $1/\sqrt{N}$.

With these approximations, the dynamics of the membrane potential Eq. (8) can be rewritten as

$$\tau \frac{\partial V_i}{\partial t} = -V_i + g_c\langle V\rangle(t) + \beta\tau\nu(t) + \mu_{ext} + \sigma\sqrt{\tau}\eta_i(t) \tag{11}$$

Equivalently, the system can be described by the probability density function (PDF) $P(V, t)$, giving the likelihood of finding a neuron at a membrane potential V at time t. From Eq. (11) the dynamics of $P(V, t)$ are given by the following Fokker–Planck equation (Risken 1984):

$$\tau \frac{\partial P(V,t)}{\partial t} = \frac{\partial}{\partial V}\left[\left(V - g_c\langle V\rangle - \beta\tau\nu(t) - \mu_{ext}\right)P(V,t)\right] + \frac{\sigma^2}{2}\frac{\partial^2}{\partial V^2}P(V,t) \tag{12}$$

The emission of a spike at the threshold imposes the following boundary conditions:

$$P(V_{th}, t) = 0, \tag{13}$$

$$\frac{\partial P}{\partial V}(V_{th}, t) = -\frac{2\nu(t)\tau}{\sigma^2}, \tag{14}$$

$$P(V_r^+, t) - P(V_r^-, t) = 0 \tag{15}$$

$$\frac{\partial P}{\partial V}(V_r^+, t) - \frac{\partial P}{\partial V}(V_r^-, t) = -\frac{2\nu(t)\tau}{\sigma^2}. \tag{16}$$

Moreover, $P(V, t)$ must obey at all times t

$$\int_{-\infty}^{V_{th}} P(V,t)dV = 1 \tag{17}$$

$$\int_{-\infty}^{V_{th}} V P(V,t)dV = \langle V\rangle(t) \tag{18}$$

Combining Eqs. (18) and (12) we obtain an evolution equation for the mean membrane potential $\langle V \rangle$:

$$\tau \frac{d\langle V \rangle}{dt} = (g_c - 1)\langle V \rangle + \mu_{ext} + [\beta - (V_{th} - V_r)]\tau \nu(t) \tag{19}$$

Note that Eq. (19) relates $\langle V \rangle$ and $\nu(t)$ in a linear manner, so that the current $g_c\langle V \rangle + \beta\tau\nu(t)$ is simply a linearly-filtered version of the incoming firing rate $\nu(t)$. Equation (19) in fact shows that the interaction term $\langle V \rangle$ is equivalent to models of chemical synapses with instantaneous rise time and exponential decay time with time constant $\tau/(1 - g_c) = \tau_m$, which can be excitatory or inhibitory depending on whether $\beta - (V_{th} - V_r)$ is positive or negative. In absence of firing ($\nu = 0$), the only effect of the sub-threshold electrical coupling is to effectively reduce the noise received by the neurons, as can be seen in terms of original notations from Eq. (7).

In the following, we first determine the properties of the asynchronous state of the network, and then examine its linear stability as function of the parameters $(\mu_{ext}, \sigma, g_c, \beta)$.

3.1 Asynchronous state

If the amplitude σ of input noise is sufficiently large, we expect to find the network in a state where neurons fire in an asynchronous manner, so that the activity of the network is invariant in time for a constant external input (μ_{ext}, σ). This asynchronous state thus corresponds to time-independent solutions of Eq. (12) with boundary conditions (13–18), which are given by Brunel and Hakim (1999), Brunel (2000)

$$P_0(V) = 2\frac{\nu_0\tau}{\sigma}\exp\left(-\frac{(V - \mu_{tot})}{\sigma^2}\right) \times \int_{\frac{V_r - \mu_{tot}}{\sigma}}^{\frac{V_{th} - \mu_{tot}}{\sigma}} \Theta\left(u - \frac{V_r - \mu_{tot}}{\sigma}\right) e^{u^2} du \tag{20}$$

where $\mu_{tot} = g_c V_0 + \beta\tau\nu_0 + \mu_{ext}$, and $\Theta(x)$ denotes the Heaviside function. The stationary firing rate ν_0 and mean membrane potential V_0 are unknown at this stage; they are obtained from Eq. (20) using the conditions (17) and (18). Equation (18) yields

$$V_0 = \frac{\mu_{ext} + \tau\nu_0(\beta + V_r - V_{th})}{1 - g_c} \tag{21}$$

so that

$$\mu_{tot} = \frac{\mu_{ext} + \tau\nu_0(\beta - g_c(V_{th} - V_r))}{1 - g_c} \tag{22}$$

The normalization condition Eq. (17) then gives an implicit equation for the stationary firing rate ν_0:

$$\frac{1}{\nu_0} = 2\tau \int_{\frac{V_{th} - \mu_{tot}}{\sigma}}^{\frac{V_r - \mu_{tot}}{\sigma}} du e^{u^2} \int_{-\infty}^{u} dv e^{-v^2} = 1/\Phi(\mu_{tot}) \tag{23}$$

where Φ is the usual transfer function of the leaky integrate-and-fire neuron (Tuckwell 1988; Amit and Brunel 1997).

Figure 2 shows the solutions ν_0 of Eq. (23), as function of μ_{ext} for different values of (g_c, β). As suggested by Eq. (22), the subthreshold coupling parameter g_c mainly acts on the input current in a multiplicative fashion. The spike-transmission parameter β determines the gain of the network for large inputs.

The firing rate predicted by Eq. (23) will be observed only if the stationary state is stable. If an instability develops, the firing rates obtained from the stationary state do not correspond to actual network dynamics. In particular, as in the case of chemically interacting neurons, if excitation predominates, i.e. β is large in comparison with $g_c(V_{th} - V_r)$, Eq. (23) predicts a region of bistability where two asynchronous states of different firing rates could coexist. This bistability is however never observed due to an oscillatory instability.

3.2 Oscillatory instabilities

To determine the linear stability of the stationary, asynchronous state described in Section 3.1, we examine the

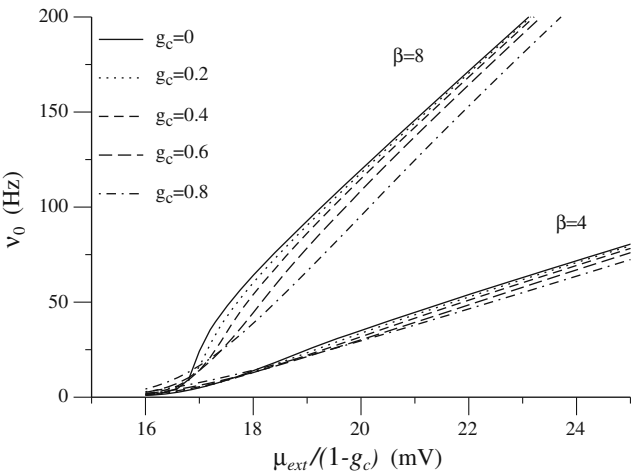

Fig. 2 Stationary firing rate ν_0 as function of the input μ_{ext} for various values of the interaction parameters g_c and β, obtained from Eq. (23) for $\sigma = 2$ mV. Here and in the rest of this study, we used $\tau_m = c_m/g_m = 20$ ms, $V_r = 10$ mV, and $V_{th} = 20$ mV. Note that the x-axis variable $\mu_{ext}/(1 - g_c)$ is simply equal to I_{ext}/g_m in the original notations (see Eq. (6))

behavior of small amplitude, time-dependent perturbations around it. If the amplitude of any perturbation decays in time, the asynchronous state is stable; on the opposite, if the amplitude of some perturbation increases in time, the asynchronous state is unstable and the network exhibits more complex dynamics. Our aim is to find the stability boundary as function of input parameters (μ_{ext}, σ) and coupling parameters (β, g_c). Here we only present the main results, the details of the calculation can be found in Appendix B.

We consider perturbations around the stationary state $(P_0(V), \nu_0, V_0)$ of the form

$$P(V,t) = P_0(V) + P_1(V,t) \tag{24}$$

$$\nu(t) = \nu_0 + \nu_1(t) \tag{25}$$

$$\langle V(t) \rangle = V_0 + V_1(t) \tag{26}$$

After expanding $P_1(V,t)$, $\nu_1(t)$ and $V_1(t)$ in eigenmodes of the form $\tilde{P}_\lambda e^{\lambda t/\tau}$, $\tilde{\nu}_\lambda e^{\lambda t/\tau}$ and $\tilde{V}_\lambda e^{\lambda t/\tau}$, we determine the complex eigenvalues $\{\lambda\}$. From Eq. (12) with conditions (13–18) we derive the following equation for these eigenvalues:

$$R_g(\lambda) R_n(\lambda) = 1. \tag{27}$$

Here R_n and R_g are both complex-valued functions.

The function R_n in Eq. (27) is the so-called firing rate response of a LIF neuron to an oscillatory input (Brunel and Hakim 1999; Brunel et al. 2001; Brunel and Hansel 2006), and is given by

$$R_n(\lambda) = \frac{\tau \nu_0}{\sigma} \frac{1}{1+\lambda} \frac{\frac{\partial U}{\partial y}(y_{th}, \lambda) - \frac{\partial U}{\partial y}(y_r, \lambda)}{U(y_{th}) - U(y_r)} \tag{28}$$

where $y_{th} = \frac{V_{th}-\mu}{\sigma}$, $y_r = \frac{V_r-\mu}{\sigma}$, and the function U is defined in Appendix B. The response function R_n has been studied in detail previously (Brunel and Hakim 1999, 2008; Brunel and Hansel 2006), as it determines the onset of oscillations in networks of neurons coupled via chemical synapses. Note that it is independent of the coupling parameters g_c and β, and, in fact, depends only on the stationary rate ν_0 and amplitude of noise σ (as well as V_{th} and V_r). Figure 3 displays the phase Φ_n and amplitude A_n of $R_n(i\omega/2\pi\tau)$ for fixed ν_0 and different values of the noise amplitude σ. For small σ, $R_n(i\omega/2\pi\tau)$ displays resonances (zeros of the phase and maxima of the amplitude) at frequencies close to multiples of ν_0; as σ is increased, the resonances are smoothed out and R_n essentially becomes a low-pass filter. For large ω, it behaves asymptotically as $e^{-\frac{i\pi}{4}}/\sqrt{\omega}$.

The function R_g in Eq. (27) is the linear filter between the incoming firing rate $\nu(t)$ and the total interaction current. It is given by

$$R_g(\lambda) = \beta + \frac{g_c[\beta - (V_{th} - V_r)]}{(1 - g_c + \lambda)}. \tag{29}$$

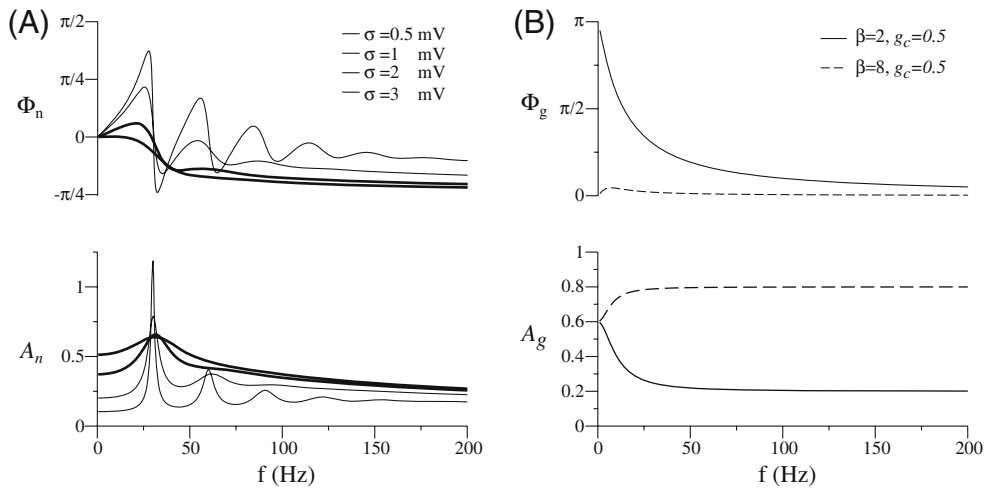

Fig. 3 Phase and amplitude of R_n and R_g as function of oscillation frequency $f = \omega/2\pi\tau$. (**A**) The rate-response function R_n depends only on the stationary firing rate ν_0 and the amplitude of noise σ. It is shown here for $\nu_0 = 30$ Hz, and four different values of σ. At low noise, R_n displays resonances: for frequencies close to multiples of ν_0, its phase Φ_n is zero and its amplitude reaches a maximum. As the noise is increased, the resonances are smoothed out, and at large noise R_n is essentially a low pass filter of amplitude decreasing as $1/\sqrt{\omega}$ and phase reaching $-\frac{\pi}{4}$ for large ω. (**B**) The function R_g depends only on the interaction parameters g_c and β. In particular, the sign of $\beta - g_c(V_{th} - V_r)$ determines its qualitative behavior. For $\beta - g_c(V_{th} - V_r) > 0$, the phase Φ_g increases from zero to a maximum value, and then decreases back to zero, while the amplitude A_g is strictly increasing. For $\beta - g_c(V_{th} - V_r) > 0$, Φ_g decreases monotonically from π to zero, and A_n is also a decreasing function

R_g depends only on the interaction parameters g_c and β (as well as V_{th} and V_r); its phase and amplitude are displayed in Fig. 3. Note that its qualitative behavior drastically depends on the sign of $\beta - g_c(V_{th} - V_r)$. Note moreover that R_g is constant $R_g = \beta$ in the absence of subthreshold coupling ($g_c = 0$). In this case, from Eq. (27) we recover the condition for the onset of oscillations in networks of purely excitatory ($\beta > 0$) or inhibitory ($\beta < 0$) neurons with instantaneous synaptic transmission (Brunel and Hakim 1999; Brunel and Hansel 2006 in the limit of zero synaptic delay).

Equation (27) is the central equation of our analysis, as its solutions determine the stability of the asynchronous state. For fixed input parameters (μ_{ext}, σ) and coupling parameters (β, g_c), if all λ solutions of Eq. (27) have a negative real part, the asynchronous state is stable; on the other hand if at least one solution of Eq. (27) has a positive real part, the asynchronous state is unstable. The stability boundaries of the asynchronous state correspond to hypersurfaces in $(\mu_{ext}, \sigma, \beta, g_c)$ on which Eq. (27) allows purely imaginary solutions $\lambda = i\omega_c$. On this boundary, the network undergoes a Hopf bifurcation, and a new oscillatory state emerges, with an oscillation frequency given by $\omega_c/2\pi\tau$.

To determine the instability boundaries in the four-dimensional parameter space $(\mu_{ext}, \sigma, \beta, g_c)$, we look for the instability line in the (μ_{ext}, σ) plane for different values of (β, g_c). Writing $R_n(i\omega) = A_n(\omega)e^{i\Phi_n(\omega)}$ and $R_g(i\omega) = A_g(\omega)e^{i\Phi_g(\omega)}$, for a given value of μ_{ext} we solve the equations

$$\Phi_n(\omega) + \Phi_g(\omega) = 0 \tag{30}$$

$$|A_n(\omega)||A_g(\omega)| = 1 \tag{31}$$

for σ and ω, which yields the instability location σ_c as well as the oscillation frequency $\omega_c/2\pi\tau$.

Once the instabilities of the asynchronous state are found by solving Eqs. (30–31), it remains to be checked whether the oscillatory state which emerges at the bifurcation is stable or not, in other words whether the bifurcation is supercritical or subcritical. This can be done in a standard manner by computing higher order terms in the expansion around the stationary state (Brunel and Hakim 1999). The analysis yields a reduced equation for the amplitude $\hat{n}_1$ of the oscillations

$$\tau \frac{d\hat{n}_1}{dt} = A\hat{n}_1 - B|\hat{n}_1|^2\hat{n}_1 \tag{32}$$

where A and B are complex numbers. Their full expression is given in Appendix B. If the real part of B is positive, the oscillatory state which appears above the bifurcation is stabilized by the non-linear term in Eq. (32), so that the bifurcation is supercritical: the amplitude of the oscillation grows continuously from zero with the distance from the instability line. On the contrary, if the real part of B is negative, the oscillatory state which appears at the bifurcation is unstable, so that the asynchronous state loses stability to another state which can not be obtained from the linear analysis.

To complement our analytical predictions on the location of the bifurcation and its nature, we perform direct numerical simulations of the network. The degree of synchrony in the network can be characterized using the (normalized) autocorrelation $C(t)$ of the instantaneous population firing rate $\nu(t)$

$$C(t) = \frac{1}{\nu_0^2}\langle \nu(t_0)\nu(t_0 + t)\rangle \tag{33}$$

If the network is in the asynchronous state, $C(t)$ is constant and equal to one. On the contrary, if the network oscillates, $C(t)$ shows maxima at zero time lag and at values corresponding to multiples of the oscillation frequency. We thus use $C(0)$ as an index of synchrony. In practice, for networks of finite size, the autocorrelation shows maxima even in the asynchronous regime, but their amplitude decreases with increasing system size.

Combining analytic and numerical results, we find that the nature of the bifurcation depends on the coupling parameters (β, g_c), through the combination $\beta - g_c(V_{th} - V_r)$. Equation (22) shows that the sign of $\beta - g_c(V_{th} - V_r)$ determines whether the firing of a neuron increases or decreases the total coupling current, i.e. whether it acts in an excitatory or inhibitory fashion. Clearly β accounts for the fast, depolarizing part of the spike, while $g_c(V_{th} - V_r)$ quantifies the transmission of the hyperpolarization due to the reset following a spike. If $\beta - g_c(V_{th} - V_r) > 0$, the net effect of spike transmission through gap junctions is excitatory, and we find analytically that the bifurcation is super-critical. On the opposite if the net effect is inhibitory, i.e. $\beta - g_c(V_{th} - V_r) < 0$, the bifurcation is sub-critical. These two cases are discussed separately in the following. For $\beta > (V_{th} - V_r)$, a rate instability appears: as we have not taken into account a refractory period following a spike, the recurrent excitation leads to an exponentially increasing firing activity in the network. In the following, we restrict the discussion to the case $\beta < (V_{th} - V_r)$.

3.2.1 Effective excitation

For $\beta - g_c(V_{th} - V_r) > 0$, the phase of R_g increases from 0 to a maximum value Φ_g^{max}, and then decreases back to zero (cf. Fig. 3(B)). We find that the zeros of Eq. (30)

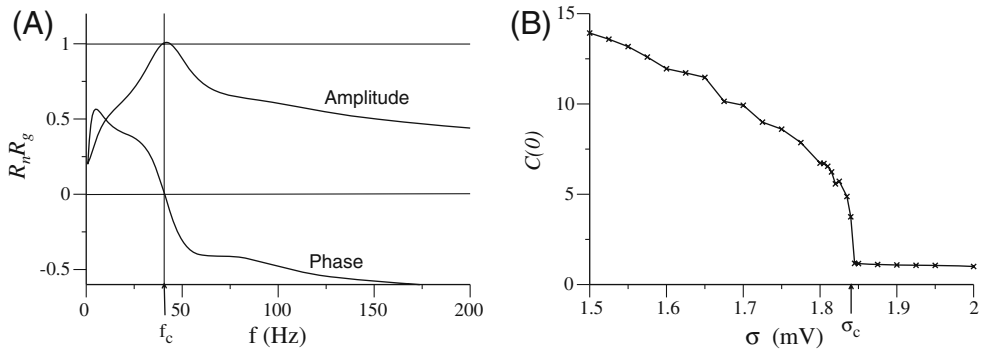

Fig. 4 Analytical prediction for the instability and direct numerical simulations for $g_c = 0.4$, $\beta = 5$ mV and $\mu_{ext} = 12$ mV. (**A**) A solution of Eqs. (30–31) is found for $\sigma_c = 1.84$ mV. The corresponding frequency $f_c = \omega_c/2\pi\tau$ is close to the resonance of R_n, i.e. close to the firing frequency ν_0 of individual neurons, here 40 Hz (on the x axis we plot $f = \omega/2\pi\tau$). (**B**) Autocorrelation at zero lag $C(0)$ of the population activity obtained from direct numerical simulations of a network of 2000 neurons. For small σ, the autocorrelation is large, indicating synchrony. As σ is increased, the autocorrelation decreases, and reaches 1 for $\sigma = 1.84$ mV, in good agreement with the analytical prediction

lie close to the zeros of Φ_n, indicating oscillations at a frequency close to the firing rate of individual neurons.

As an illustration, Figs. 4 and 5 show the instability found for $\mu_{ext} = 12$ mV, $g_c = 0.4$ and $\beta = 5$ mV. A solution of Eqs. (30–31) is found for $\sigma_c = 1.84$ mV, as seen graphically in Fig. 4(A). The corresponding oscillation frequency $\omega_c/2\pi\tau$ lies close to the maximum of A_n, and thus close to $\nu_0 = 40$ Hz. The coefficient B in Eq. (32) is found to be positive, so that the bifurcation is supercritical. The analytic value of σ_c is in excellent agreement

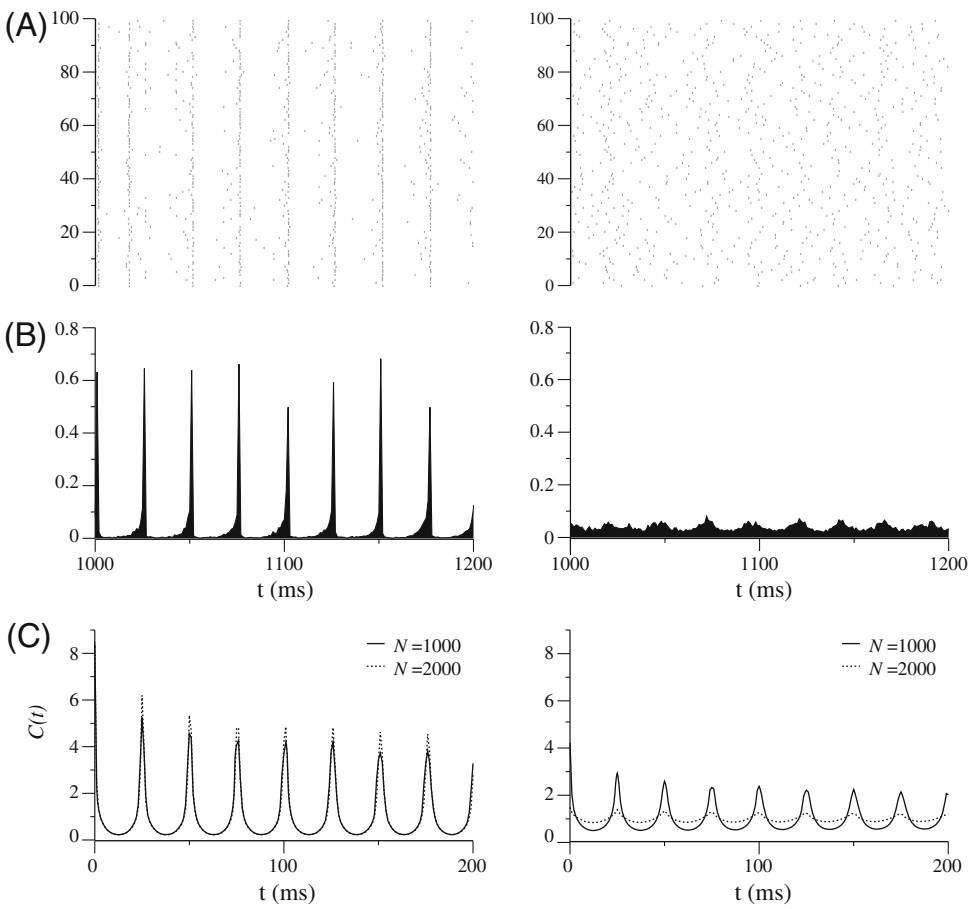

Fig. 5 Network activity on the two sides of the bifurcation, obtained from numerical simulations of a network of $N = 2000$ neurons, for the same parameters as in Fig. 4. *Left column*: $\sigma = 1.8$ mV, oscillatory state; *right column*: $\sigma = 1.85$ mV, asynchronous state. (**A**) Spike raster of a subset of 100 neurons. (**B**) Instantaneous population firing rate $\nu(t)$ computed in 1 ms bins. (**C**) Autocorrelation of the instantaneous population firing rate for two network sizes, $N = 1000$ and $N = 2000$ neurons. Due to finite-size effects, the autocorrelation is not flat above σ_c (*right column*), but the amplitude of the oscillations decreases with system size. In contrast, below σ_c (*left column*), the amplitude of the oscillations increases with the system size

with numerical simulations, as seen in Fig. 4(B), where the autocorrelation at zero lag is displayed as function of σ. Figure 5 displays the activity of the numerically simulated network on the two sides of the bifurcation. As seen from the raster plots and the population firing rate $\nu(t)$, in the oscillatory state the majority of neurons fire in tight synchrony, which agrees with the prediction that the oscillation frequency of the network is close to the firing rate of individual neurons.

The full phase diagram in the (μ_{ext}, σ) plane is displayed in Fig. 6. For fixed, suprathreshold input current, the asynchronous state is stable for large σ; for small σ the network is in an oscillatory state in which all neurons fire in precise synchrony. For all values of β and g_c examined, the bifurcation is found to be supercritical (provided $\beta - g_c(V_{th} - V_r) > 0$).

The critical value σ_c at which the bifurcation occurs increases with β. For small and moderate values of β, the oscillation frequency at the bifurcation is very close to the firing rate of individual neurons, i.e. $w_c/2\pi\tau = \nu_0$, so that the neurons fire synchronously and regularly. As β is increased to values close to $V_{th} - V_r$, the oscillation frequency decreases with respect to ν_0, so that at large β at the instability the network activity shows oscillations while the individual neurons fire irregularly: this is an instance of synchronous irregular state (Brunel 2000) with *low* oscillation frequencies.

As seen in Fig. 6, as long as $\beta - g_c(V_{th} - V_r) > 0$, the subthreshold coupling parameter g_c has very little effect other than shifting the threshold for the input current. Qualitatively, for $g_c \neq 0$, the phase diagram is thus essentially the same as that for $g_c = 0$, which corresponds to a network coupled via instantaneous, excitatory synapses of strength β.

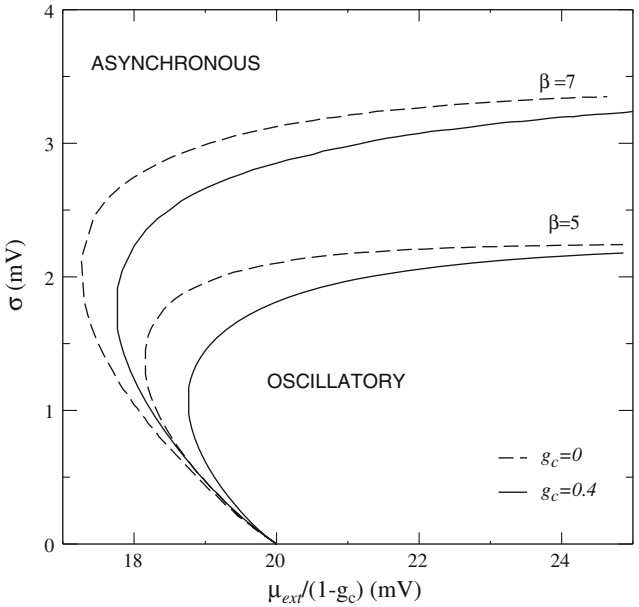

Fig. 6 Phase diagram of network dynamics in the plane $(\mu_{ext}/(1-g_c), \sigma)$, for the case $\beta - g_c(V_{th} - V_r) > 0$. The instability lines were determined from Eqs. (30–31) for different values of interaction parameters (β, g_c). The asynchronous state is stable for σ large and μ_{ext} small. Its stability boundary depends strongly on the value of β, and weakly on the value of g_c. Instability lines corresponding to different values of g_c are displayed with different symbols. Note that the x-axis variable $\mu_{ext}/(1-g_c)$ is simply equal to I_{ext}/g_m in the original notations (see Eq. (6)). To obtain the phase diagram in original notations Δ versus I_{ext} it is therefore sufficient to divide the y-values by $\sqrt{1-g_c}$ (see Eq. (7))

3.2.2 *Effective inhibition*

For $\beta - g_c(V_{th} - V_r) < 0$, the phase Φ_g of R_g decreases monotonically from π to zero (cf. Fig. 3(B)). In consequence, the zeros of $\Phi_g + \Phi_n$ are significantly distinct from those of Φ_n alone, and the predicted stability boundary looks qualitatively different from the case of effective excitation. In particular, the predicted values of the oscillation frequency at the bifurcation are now always *larger* than the firing rates of individual neurons, and possibly very large. This is illustrated in Fig. 7(A) for $\mu_{ext} = 11.5$, $g_c = 0.5$, $\beta = 2$: a solution of Eqs. (30–31) is found for $\sigma_c = 0.4$ mV, and the corresponding oscillation frequency $\omega_c/2\pi\tau$ lies above the second peak of A_n, i.e. $\omega_c/2\pi\tau = 80$ Hz, while $\nu_0 = 38$ Hz. Close to the transition, we would thus expect to find the network in synchronous irregular state with a fast oscillation frequency (Brunel and Hakim 1999; Brunel 2000). Calculating the coefficient B in Eq. (32) (see Appendix B) however predicts that the bifurcation is subcritical, so that this oscillatory state is unstable.

Direct numerical simulations in which σ was progressively decreased from a large value indeed display a sharp transition close to the predicted instability point. Crossing σ_c from above, the network switches abruptly from the asynchronous state to a fully synchronous one. This observed synchronous state corresponds to an oscillatory state not captured by the linear analysis, and whose stability extends up to a larger value of noise. Indeed, increasing progressively the value of σ from 0, we find no sign of transition at σ_c, but instead at a larger value σ_s, as shown in Fig. 7(B). Such a hysteresis is typical for a subcritical Hopf bifurcation. It implies that between σ_c and σ_s the network exhibits bistability, both the asynchronous and the synchronous states being stable; the asynchronous state loses stability as σ_c is crossed from above, while the synchronous state loses stability as σ_s is crossed from below.

At any value of σ between σ_c and σ_s, the network can be found either in the asynchronous or in the

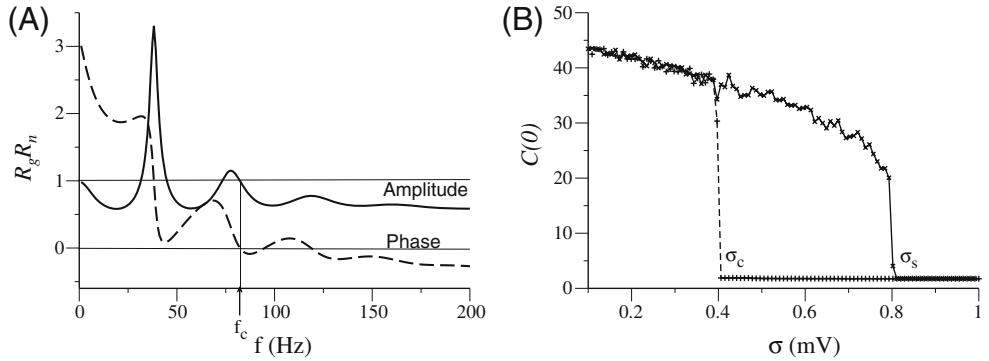

Fig. 7 Analytical prediction for the instability and direct numerical simulations for $g_c = 0.5$, $\beta = 2$ mV and $\mu_{ext} = 11.5$ mV. (**A**) A solution of Eqs. (30–31) is found for $\sigma = 0.4$ mV. The corresponding frequency $f_c = \omega_c/2\pi\tau$ is close to the second peak of A_n, i.e. close to twice the firing frequency ν_0 of individual neurons (on the x axis we plot $f = \omega/2\pi\tau$). (**B**) Autocorrelation at zero lag of the population activity obtained from direct numerical simulations. The autocorrelation exhibits an hysteresis depending on whether the noise amplitude σ is increased or decreased. If σ is progressively increased from zero, the autocorrelation remains large until $\sigma_s = 0.8$ mV, at which point the synchronous state abruptly loses stability. If σ is decreased progressively from a large value, the autocorrelation remains close to 1 until the analytically predicted value $\sigma_c = 0.4$ mV. In between σ_c and σ_s, the network exhibits bistablity between a fully synchronous and the asynchronous state

synchronous state, depending on its history. These two states are illustrated in Fig. 8, where we show the activity in a network of 2000 neurons, for a given set of parameters, but two different initial conditions leading to the synchronous and the asynchronous state. For networks of small numbers of neurons, the fluctuations in the coupling current mediated by the gap junctions are large and can induce spontaneous transitions between the two stable states in a random fashion, as illustrated in Fig. 9. In that case the population firing rate, which corresponds to the experimentally accessible local field potential, alternates between strong oscillations and uniform activity in an intermittent fashion.

The full phase diagrams in the (μ_{ext}, σ) plane are displayed in Fig. 10, where we show for several values of the interaction parameters the analytically determined stability boundary of the asynchronous state, and the numerically obtained stability boundary of the synchronous state. Analytically, the bifurcation is found to be subcritical for any value of μ_{ext}. Numerical simulations however show that the bistability region is the largest for currents of intermediate values, and becomes very small for μ_{ext} large. The total size of the bistable region increases as $\beta - g_c(V_{th} - V_r)$ is decreased, indicating that the inhibitory effect of spike transmission via electrical coupling favors bistability. For a given value of g_c,

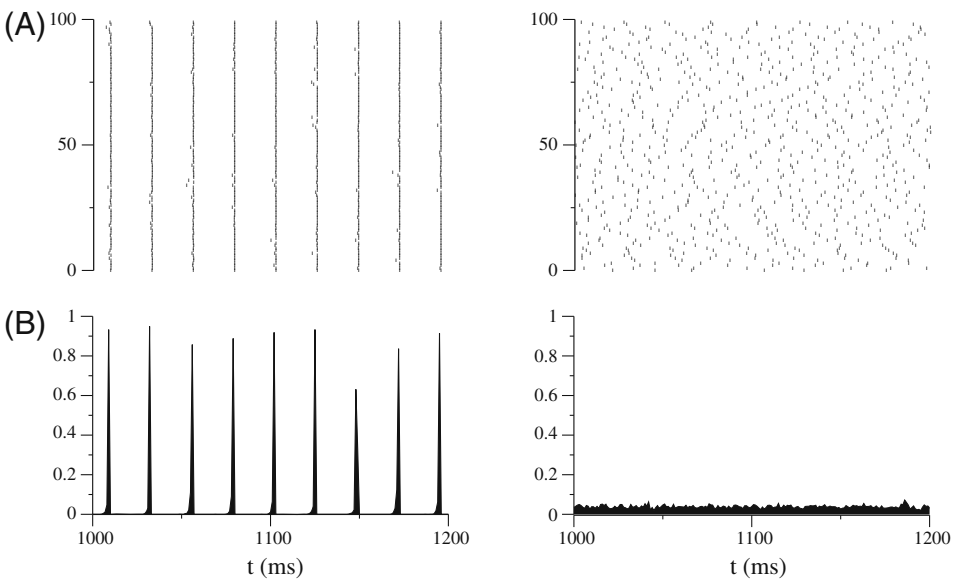

Fig. 8 Network activity in the two stable states for $\sigma = 0.6$ mV, obtained from numerical simulations of a network of $N = 2000$ neurons. All other parameters are identical to Fig. 7. Left column: synchronous state; right column: asynchronous state. (**A**) Spike raster of a subset of 100 neurons. (**B**) Instantaneous population firing rate $\nu(t)$ computed in 1 ms bins

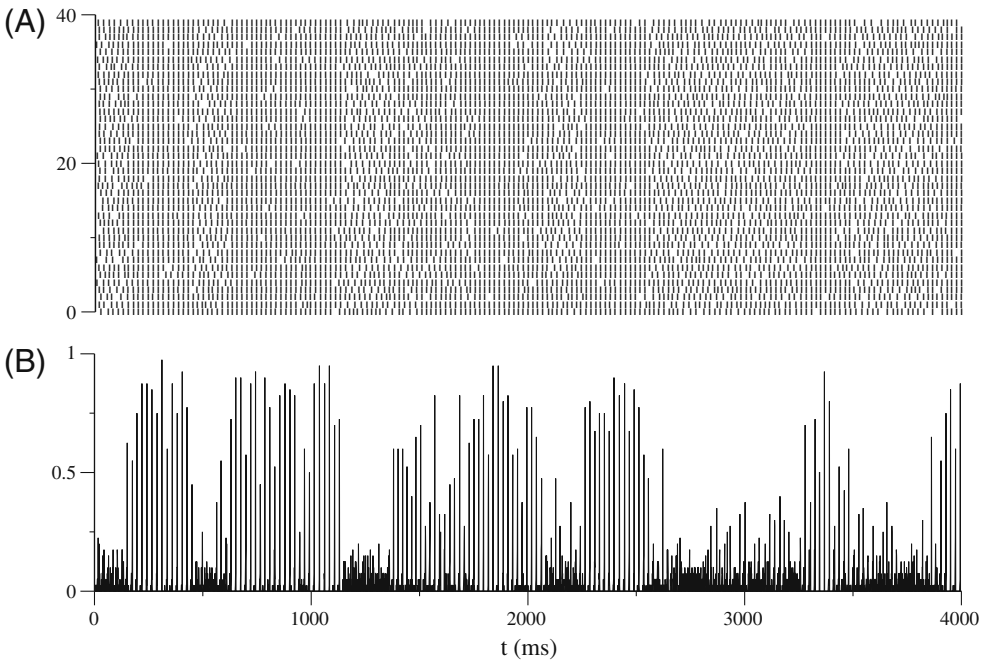

Fig. 9 Bistability in a network of $N = 40$ neurons for $\sigma = 0.7$ mV, all other parameters being identical to Fig. 7. (**A**) spike raster of the full network; (**B**) instantaneous population firing rate $\nu(t)$ computed in 1 ms bins. In such a small system, the fluctuations in the total coupling current received by each neuron are large, so that the network keeps on switching between the asynchronous and the synchronous state. In consequence, the total population firing rate shows an intermittent behavior between strong oscillations and more uniform activity

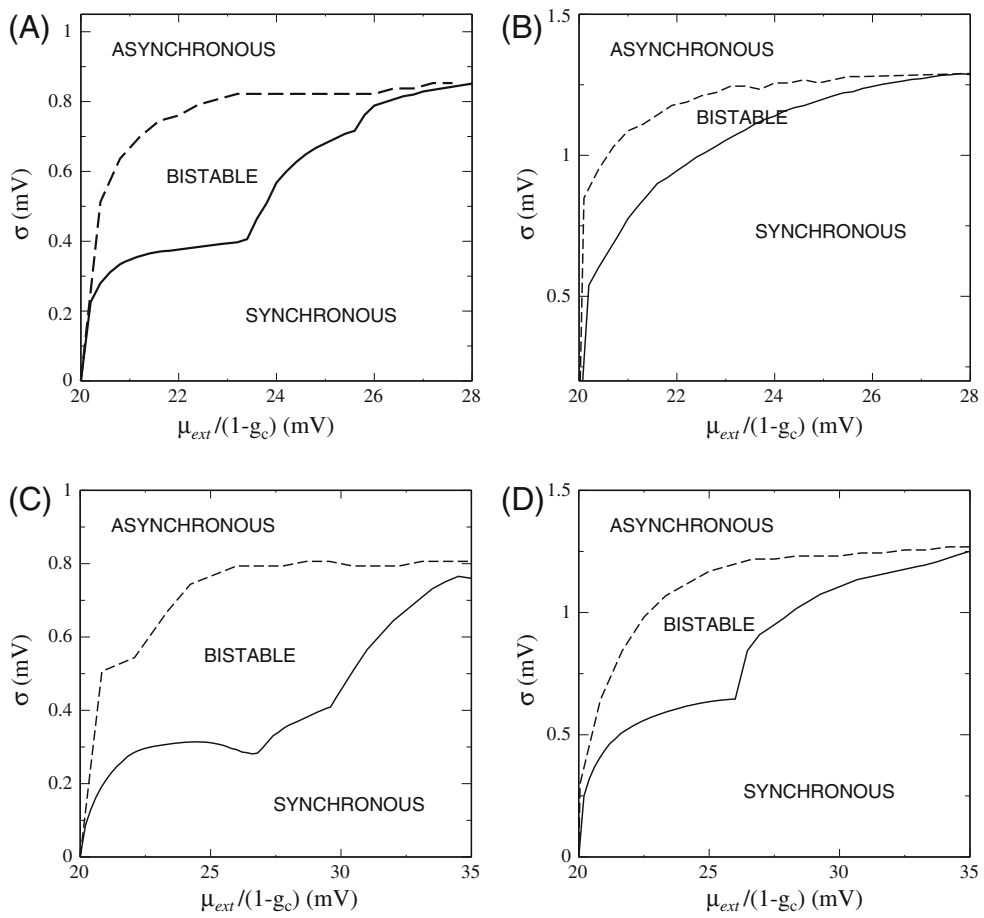

Fig. 10 Phase diagram of network dynamics in the plane $(\mu_{ext}/(1-g_c), \sigma)$, for the case $\beta - g_c(V_{th} - V_r) < 0$. (**A**) $\beta = 2\ mV$, $g_c = 0.5$; (**B**) $\beta = 3\ mV$, $g_c = 0.5$; (**C**) $\beta = 2\ mV$, $g_c = 0.7$; (**D**) $\beta = 3\ mV$, $g_c = 0.7$. The analytically determined instability line is displayed in solid, it corresponds to the stability boundary of the asynchronous state, which is stable at large σ. The instability line obtained numerically by progressively increasing σ from zero is displayed as a dashed line. It corresponds to the stability limit of the synchronous state which is stable for small σ. Between these two lines, the network is bistable. Note that the x-axis variable $\mu_{ext}/(1-g_c)$ is simply equal to I_{ext}/g_m in the original notations (see Eq. (6)). To obtain the phase diagram in original notations Δ versus I_{ext} it is therefore sufficient to divide the y-values by $\sqrt{1-g_c}$ (see Eq. (7))

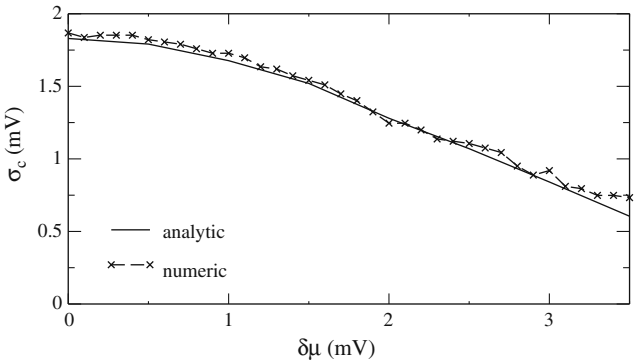

Fig. 11 Effect of the heterogeneity on the boundary between the synchronous and the asynchronous state in the case of effective excitation. The amplitude of the noise σ_c at the bifurcation is plotted as function of the range $\delta\mu$ of input currents, for $\bar{\mu}_{ext} = 12$ mV, $\beta = 5$ mV and $g_c = 0.4$. *Full line*: analytical prediction, crosses: numerical results

if β is increased, the bistable region is shifted to higher values of noise, but its total area decreases.

4 Analysis of network dynamics: heterogeneous case

So far, we have investigated homogeneous networks, in which the properties of all neurons are identical and the coupling between any two neurons is the same. This is a drastic simplification in comparison with the physiological situation, where any characteristic property is typically found to exhibit a range of values in a neuronal population. The main effect of such heterogeneity is that different neurons in the network fire at different mean rates, so that it becomes much more difficult for the network to synchronize. Here we investigate quantitatively the effects of heterogeneity on the network dynamics, and examine the robustness of the phase diagrams obtained in Section 3.

To introduce heterogeneity in a simple fashion, we consider the situation in which the input currents $\mu_{ext,i}$ to different cells are not anymore identical, but distributed randomly from a distribution η of mean $\bar{\mu}_{ext}$ and width $\delta\mu$. All other parameters are identical for all neurons, although the effect of their heterogeneity could easily be taken into account within a similar approach. This case can be studied analytically following the same main steps as in Section 3. Details of the calculation can be found in Appendix C.

As a consequence of the heterogeneity of the input currents, the firing rates of the individual neurons in the asynchronous state are not all identical, but distributed with a distribution $\rho(\nu)$. The equation for the instability Eq. (27) now becomes

$$R_g(i\omega)\bar{R}_n(i\omega) = 1. \tag{34}$$

where $\bar{R}_n(i\omega) = \int d\nu \rho(\nu) R_n(i\omega, \nu)$, i.e. $\bar{R}_n(i\omega)$ is simply the average of the rate-response functions $R_n(i\omega, \nu)$ over the distribution of firing rates present in the network.

We studied in detail the particular case in which the input currents are distributed uniformly within $[\bar{\mu}_{ext} - \delta\mu, \bar{\mu}_{ext} + \delta\mu]$. Such an input distribution leads, in the asynchronous state, to a distribution of firing frequencies which is approximately uniform around the mean network firing frequency $\bar{\nu}_0 = \Phi(\bar{\mu}_{ext})$ (cf. Fig. 13(C)), Φ being the f-I function defined in Eq. (23). The effect of the heterogeneity on the location of the Hopf bifurcation was examined separately for the cases where the effective spike transmission is excitatory and inhibitory.

In the excitatory case, the Hopf bifurcation was found to be supercritical in the homogeneous system.

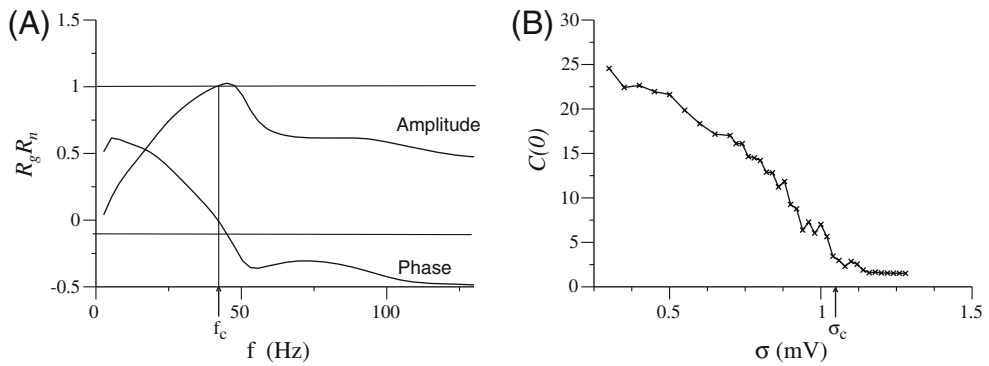

Fig. 12 Analytical prediction for the instability and direct numerical simulations for $\mu_{ext} = 12$ mV, $\beta = 5$ mV, $g_c = 0.4$ and $\delta\mu = 2.5$ mV. (**A**) A solution of Eqs. (30–31) is found for $\sigma_c = 1.05$ mV. The corresponding oscillation frequency is $f_c = \omega_c/2\pi\tau = 40$ Hz, as in the homogeneous case, although the overall shape of the phase and amplitude are different (cf. Fig. 4) (**B**) Autocorrelation at zero lag $C(0)$ of the population activity obtained from direct numerical simulations of a network of 2000 neurons

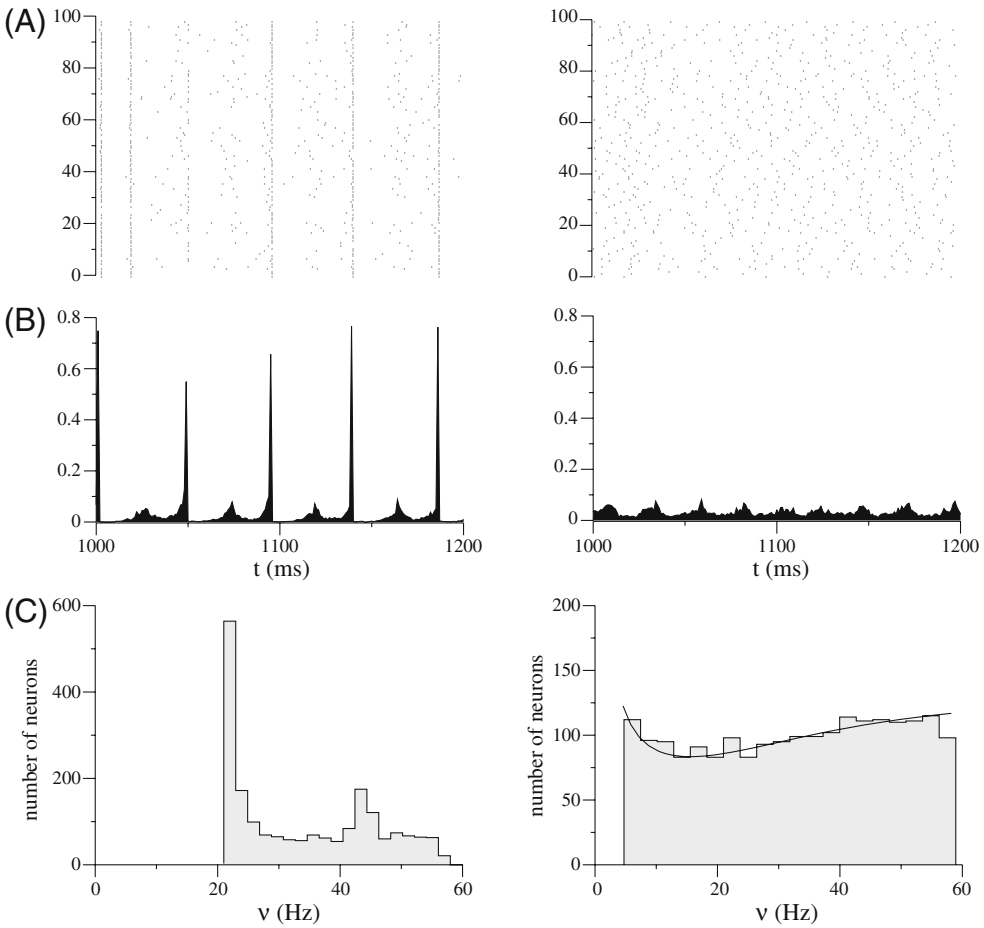

Fig. 13 Network activity on the two sides of the bifurcation, obtained from numerical simulations of a network of $N = 2000$ neurons, for the same parameters as in Fig. 12. *Left column*: $\sigma = 0.8$ mV, oscillatory state; *right column*: $\sigma = 1.1$ mV, asynchronous state. (**A**) Spike raster of a subset of 100 neurons. (**B**) Instantaneous population firing rate $\nu(t)$ computed in 1 ms bins. (**C**) Distribution of mean firing rates in the network. The *bold line* represents the analytic prediction obtained from Eq. (105), and the histogram displays results of simulations

By comparing analytical predictions with numerical simulations, we found that the bifurcation remains supercritical in presence of heterogeneities. Figure 11 displays the critical noise amplitude σ_c as function of the heterogeneity strength $\delta\mu$. As could be expected, σ_c decreases as $\delta\mu$ is increased, but the decrease is rather slow, so that σ_c remains non-zero for large heterogeneities. As an illustration, Figs. 12 and 13 show that for $\delta\mu = 2.5$, $\sigma_c = 1$ mV, while the firing rates are distributed uniformly between 10 and 60 Hertz. Although our calculation predicts correctly the location of the instability, note that it fails to predict the oscillation frequency: in the example shown in Fig. 13, the oscillatory state reached after the bifurcation consists of two clusters oscillating respectively at 25 and 50 Hertz. The precise number of clusters reached in the synchronous state depends on the shape of the distribution of input currents: in the case of a gaussian, the synchronous state consists of a single cluster oscillating at the mean firing rate of the network.

In the parameter region where the spike transmission is inhibitory, the effect of the heterogeneity on the bistable region is illustrated in Fig. 14, where we plot the boundaries σ_c and σ_s of the bistable region as function of the amplitude of the heterogeneity $\delta\mu$, all other parameters being fixed. As $\delta\mu$ is increased, σ_c and σ_s decrease, yet the size of the bistable region

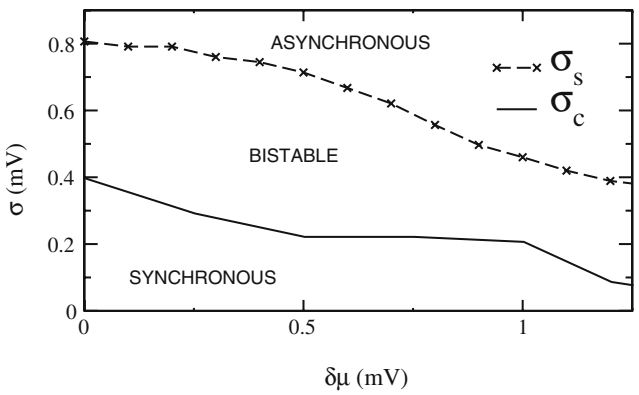

Fig. 14 Effect of the heterogeneity on the bistability: the boundaries of the bistable region σ_c and σ_s are plotted as function of the amplitude of the heterogeneity in the inputs $\delta\mu$. The other parameters are identical to Fig. 7 ($g_c = 0.5$, $\beta = 2$ mV, $\bar{\mu}_{ext} = 11.5$ mV)

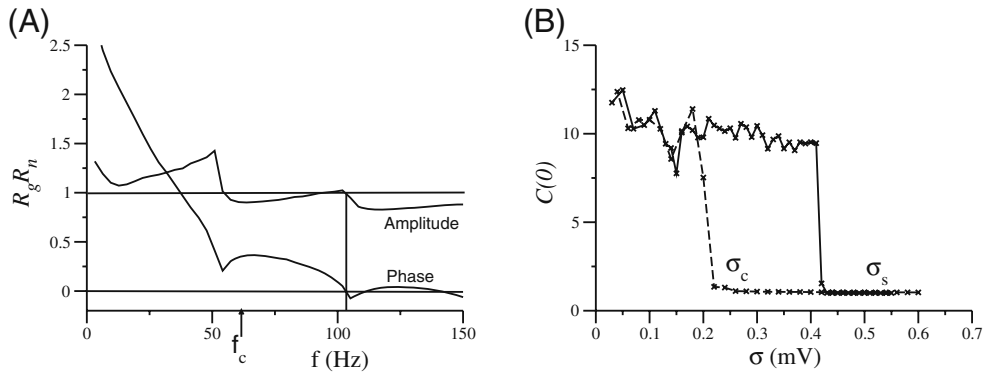

Fig. 15 Analytical prediction for the instability and direct numerical simulations for $g_c = 0.5$, $\beta = 2$ mV, $\bar{\mu}_{ext} = 11.5$ mV and . $\delta\mu = 1$ mV. (**A**) A solution of Eqs. (30–31) is found for $\sigma = 0.21$ mV (on the x axis we plot $f = \omega/2\pi\tau$). (**B**) Autocorrelation at zero lag of the population activity obtained from direct numerical simulations. The autocorrelation exhibits an hysteresis depending on whether the noise amplitude σ is increased or decreased. If σ is progressively increased from zero, the autocorrelation remains large until $\sigma_s = 0.42$ mV, at which point the synchronous state abruptly loses stability. If σ is decreased progressively from a large value, the autocorrelation remains close to 1 until the analytically predicted value $\sigma_c = 0.21$ mV

$\sigma_s - \sigma_c$ remains large for large values of $\delta\mu$. Effectively, the heterogeneity thus acts as an additional noise in the system, but does not destroy bistability. In particular, if the heterogeneity is large enough, the purely synchronous region vanishes, while the bistable region persists at small noise. Figure 15 shows the hysteresis for $\delta\mu = 1$. Note that due to the heterogeneity, the finite-size effects induce much larger fluctuations than in the homogeneous case. Figure 16 displays the activity in the two states of the corresponding bistable region

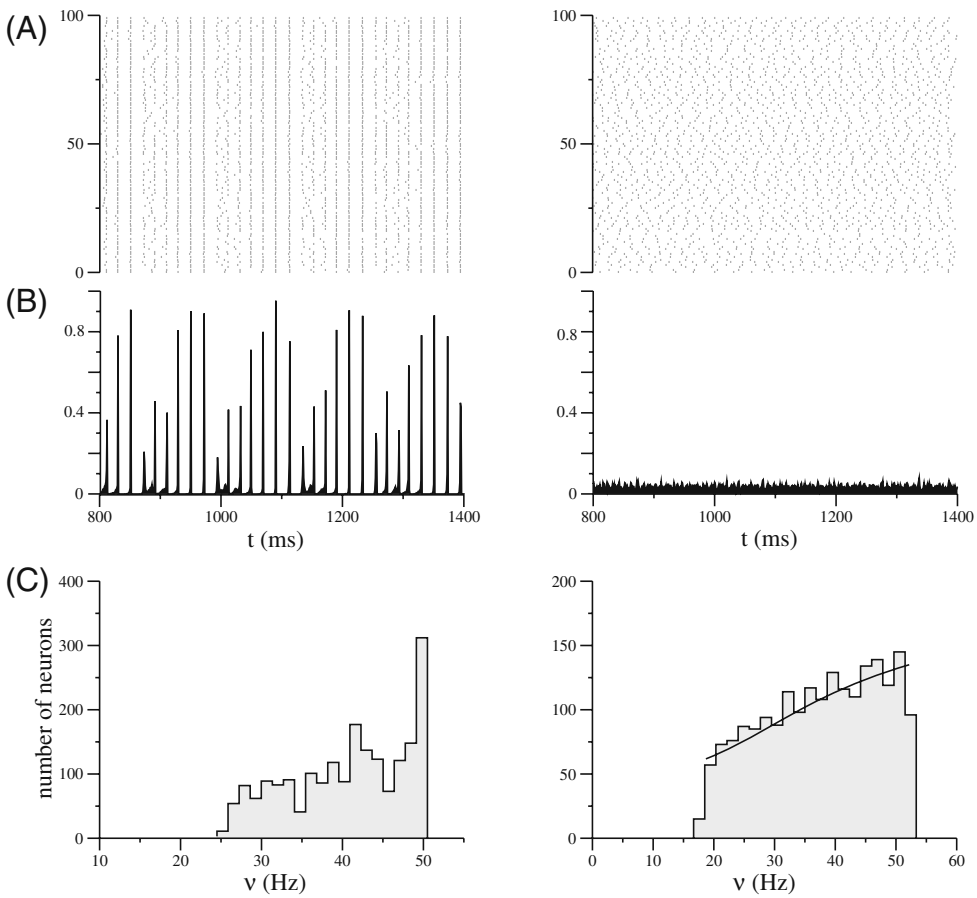

Fig. 16 Network activity in the two stable states for $\sigma = 0.3$ mV, obtained from numerical simulations of a network of $N = 2000$ neurons. All other parameters are identical to Fig. 15. *Left column*: synchronous state; *right column*: asynchronous state. (**A**) Spike raster of a subset of 100 neurons. (**B**) Instantaneous population firing rate $\nu(t)$ computed in 1 ms bins. (**C**) Distribution of mean firing rates in the network. The *bold line* represents the analytic prediction obtained from Eq. (105), and the *histogram* displays results of simulations

for $\sigma = 0.3$. In contrast to the homogeneous case, the synchronized state is not fully synchronized, but exhibits sharp bursts of synchrony. Note also that, all parameters being equal, the distribution of firing rates is narrower in the synchronized state.

5 Inducing oscillations in an asynchronous network of electrically coupled neurons

In Sections 3 and 4, we investigated how oscillations and synchrony can be generated in a network of electrically coupled neurons receiving a steady, time-independent mean input. Instead of being generated by the network itself, oscillations could also be induced in an initially asynchronous network by an external time-dependent drive. In this section, we examine two possible scenarios by which synchrony can be induced by external inputs.

5.1 Resonance in response to incoming oscillations

Supposing the network receives time-varying mean inputs, due for example to oscillations generated by a pre-synaptic network external to the one under study, a natural question is whether these oscillations are suppressed or promoted by the electrical coupling between neurons. This question can be addressed analytically in our setting when the amplitude of the time-varying component is small enough to be treated at the linear level.

We consider the case where the (homogeneous) network is in the asynchronous state, and receives inputs of the form $\mu_{ext} + \mu_1 \sin(\omega t)$, where ω is the angular frequency of the incoming oscillation, and $\mu_1 << \mu_{ext}$ is its amplitude. In response to the sinusoidal modulation of the inputs, at the linear level the mean firing rate becomes $\nu(t) = \nu_0(1 + \nu_1 \sin(\omega t + \phi))$, in other words the network starts oscillating at the frequency of input oscillations ω. The amplitude ν_1 and phase lag ϕ of network oscillations depend on ω, so that some oscillation frequencies are favored with respect to others. The expression for ν_1 and ϕ can be obtained analytically (see Appendix D), and reads:

$$\nu_1 e^{i\phi} = \frac{1}{\tau \nu_0} \frac{1 + i\omega}{1 + i\omega - g_c} \frac{1}{1 - R_g(i\omega) R_n(i\omega)} R_n(i\omega) \mu_1 \tag{35}$$

with functions R_n and R_g defined respectively in Eq. (28) and (29). Although Eq. (35) is a linear approximation in principle valid only for very small ν_1, comparison with simulations shows that it is accurate for ν_1 up to half of the mean firing frequency ν_0.

In Fig. 17, we display ν_1 and ϕ as function of $\omega/2\pi\tau$. The oscillation amplitude ν_1 displays a resonant peak for $\omega/2\pi\tau$ close to the mean firing rate ν_0. At this input frequency, the phase lag is zero, the oscillations in the network are perfectly in phase with the input. These results indicate that inputs oscillating at the frequency of the firing in the network strongly synchronize the neurons in the network.

In comparison, in an uncoupled network of same average firing rate and input noise amplitude, the resonance is much weaker. (Note that in this case, Eq. (35) reduces to $\nu_1 e^{i\phi} = R_n(i\omega)$, ie. the response is simply given by the function R_n as mentioned earlier). These results show that the coupling between neurons strongly enhances the capacity of the network to synchronize in response to oscillatory inputs.

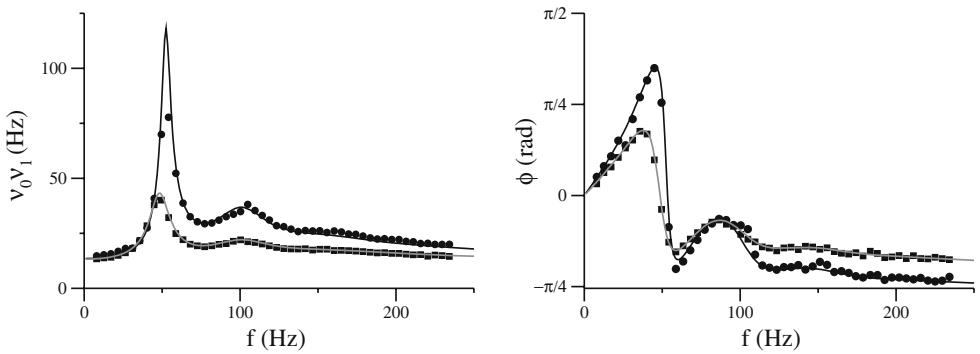

Fig. 17 Electrical coupling resonantly enhances the network firing rate response to a sinusoidally modulated current of frequency $f = \omega/2\pi\tau$. *Solid line*: response of a homogeneous network with $g_c = 0.5$, $\beta = 2$ mV, $\sigma = 1$ mV and $\nu_0 = 50$ Hz (*line*: analytical prediction; *points*: numerical results). *Grey line*: response of an uncoupled population of neurons with $\sigma = 1$ mV and $\nu_0 = 50$ Hz (*line*: analytical prediction; *points*: numerical results). The input currents were adjusted to obtain the same mean firing frequency in both cases and $\mu_1 = 1$ mV. *Left*: amplitude ν_1 as function of f; right: phase lag ϕ as function of f

5.2 Transitions between the synchronous and the asynchronous state in the bistable region

As seen in Section 3.2.2, for $\beta - g_c(V_{th} - V_r) < 0$, the system is bistable for a large range of input parameters, i.e. it exhibits two attractor states, an asynchronous and a synchronous one. In networks of small size, the fluctuations are large, and the network switches spontaneously between the two states. For larger networks, the amplitude of internal fluctuations for constant inputs is too small to lead to transitions, and in absence of external perturbations, the network remains in the state determined by its initial conditions. Here we briefly examine how external inputs can switch the network between these two states, and in particular induce synchrony.

We consider the situation in which a fraction n neurons in the network receives at time t_0 a strong, synchronous input which brings all nN neurons above threshold. As shown in Fig. 18(A), if the fraction n is large enough, the synchronous inputs can induce a transition from the asynchronous state to the synchronous one. The size of the fraction necessary for such a switch clearly depends on the relative sizes of the basins of attraction of the two states, so that it approaches 1 for σ close to σ_s, and it decreases monotonically to 0 for σ close to σ_c.

Conversely, the network can also switch from synchrony to asynchrony if a fraction of neurons fires simultaneously out of phase with the network oscillations (Fig. 18(B)). The value of the fraction necessary for this opposite switch of course depends on the value of σ, but it also depends on the precise phase of the oscillation at which this subnetwork fires synchronously, so that only a strongly out-of-phase event will disrupt the synchrony in the network.

6 Discussion

In this study we present a detailed analysis of the effects of electrical coupling on the synchronization of neuronal firing in large networks. Altogether, our results demonstrate that electrical coupling can lead to oscillatory synchrony even in presence of strong noise and heterogeneities. In contrast to inhibitory chemically-coupled networks, we find that the period of the oscillation is not determined by the time course of the inhibitory currents following a spike, but rather by the intrinsic firing rate of the neurons. In presence of heterogeneities, the synchrony can become loose, many cells skipping cycles in the oscillations, however the oscillation frequency remains tied to the mean firing rate in the network. The oscillations in the network are therefore inherently *regular* in contrast with synchronous irregular states found in networks coupled by chemical synapses (Brunel and Hakim 1999; Brunel 2000).

An important conclusion of our analysis is that the qualitative effects of electrical coupling depend critically on the shape of the action potentials. We have found qualitatively different behaviors depending on whether the effect of spike transmission via electrical coupling is predominantly excitatory or inhibitory. In real networks, we expect the (excitatory or inhibitory) nature of the coupling to be controlled by the relative weight of the depolarizing and the hyperpolarizing parts of the spikelet. The effect of the spikes should be dominantly excitatory if the spikes are slow, and their depolarizing part broad, while the hyperpolarization following the firing is small. On the other hand their effect should be inhibitory if the spikes are fast and the after-hyperpolarization large. Interestingly, these two different types of spikes are experimentally observed in

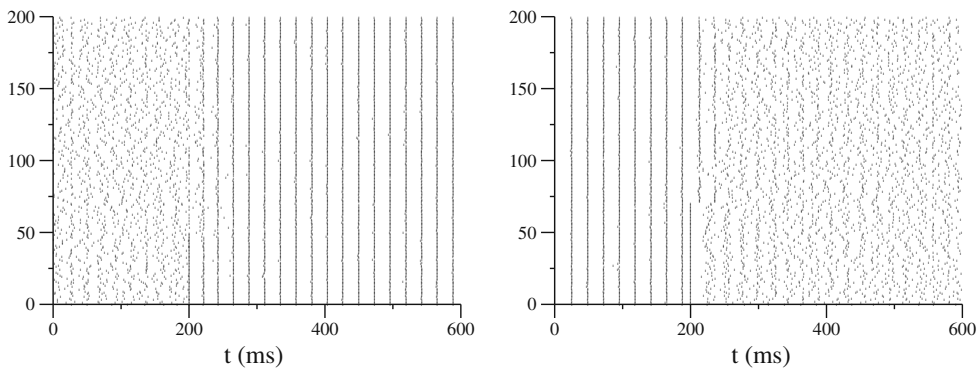

Fig. 18 Transitions between the asynchronous and the synchronous state in a network of $N = 200$ neurons, induced by the coincident firing of a subset of n neurons. At time $t = 200$ ms, n neurons are forced to fire simultaneously by increasing their membrane potential to threshold. *Left*: transition from asynchrony to synchrony after the simultaneous firing of $n = 50$ neurons; *right*: transition from synchrony to asynchrony after the simultaneous firing of $n = 70$ neurons. All parameters are identical to Fig. 8

different types of interneurons (Galarreta and Hestrin 2001a; Connors and Long 2004).

In the case where the spike transmission is dominantly excitatory, the effect of electrical coupling is found to be qualitatively similar to the effect of chemical excitatory synapses. Experimental data suggests that some inter-neurons, in particular low-threshold spiking cells (Connors and Long 2004), might belong to this class. The main difference between electrical excitatory coupling and chemical excitatory synapses is that for proximal electrical synapses, the transmission delay is typically of the order of 200 μs (Galarreta and Hestrin 2001a), and thus much shorter than in the case of chemical synapses. The consequence of this almost vanishing delay is a higher resistance of oscillations to noise, as adding a delay in our analysis would push the instability boundary to higher noise values (data not shown).

In the situation where the spike transmission is dominantly inhibitory, we find a qualitatively distinct behavior: in a large region of parameters the network dynamics display bistability between an asynchronous and a synchronous state. Although bistability between synchrony and asynchrony has been occasionally observed in some models of chemically coupled networks (Gerstner and van Hemmen 1993; Timme et al. 2002; Brunel and Hansel 2006), it was mostly restricted to small parameter ranges. In contrast, we showed here that in electrically coupled networks, bistability is a generic and robust phenomenon found in large parameter domains, and resistant to high levels of heterogeneity. It is moreover not an artifact of the simplified description of action potentials which we adopted, as it is observed also in more realistic models (see Appendix A). Bistability between synchrony and anti-synchrony has been previously found in models of pairs of identical, electrically coupled neurons in the limit of vanishing noise (Lewis and Rinzel 2003; Bem et al. 2005). In our case, the bistable region does not extend to zero noise (except at very high heterogeneity), so that the bistability we observe is not a direct correspondence of that in pairs of neurons. The absence of this correspondence is not surprising as our mean-field results could not be expected to extend to networks consisting of pairs of neurons.

Intra-cellular recordings in a variety of interneurons (Galarreta and Hestrin 1999, 2001a; Dugué et al. 2008) suggest that electrical coupling is dominantly inhibitory due to the transmission of after-hyperpolarization following action potentials. The finding that electrical synapses between such inter-neurons define highly connected, local modules has raised questions about the possible function of such modules (Hestrin and Galarreta 2005). Our model is particularly relevant for the theoretical description of such modules, and interestingly our findings support putative functional roles inferred from experiments, but also suggest additional ones. A first and most prominent function of an electrically coupled network module has been proposed to be the generation and enhancement of synchrony. Our study strongly supports this possibility: we have shown that synchrony can be internally generated by the network, but have also found that the network can strongly enhance synchrony induced by time-varying external inputs. Indeed we have seen that the electrical coupling leads to a strong resonance in the network response at frequencies close to the firing rate of the individual neurons, so that an oscillatory input would strongly synchronize the firing of the neurons.

As a second putative role, it has been suggested that an electrically coupled module could function as a detector of strong coincident inputs. Interestingly, we have found that strong coincident inputs to a subset of neurons can switch the network between the synchronous and the asynchronous attractor states in the bistable regime. In that regime, the network not only detects the occurrence of a coincident event, but also remembers the occurrence of this event until another coincident event disrupts it, and switches it back to an asynchronous state. Our study thus suggests that a module of electrically coupled neurons could serve as a short term memory of a coincident event. The functioning of such time-based attractors however needs to be investigated in a study taking into account a more complex spatial connectivity of the network.

The results presented here were obtained for fully connected networks. Experimental studied have found that electrical coupling between inhibitory cells defines networks that are locally very highly coupled, as the probability of finding a connection between two close cells ranges from 40 to 100% (Galarreta and Hestrin 1999; Gibson et al. 1999; Mann-Metzer and Yarom 1999; Beierlein et al. 2000; Landisman et al. 2002; Bennett and Zukin 2004; Connors and Long 2004; Galarreta et al. 2004; Hestrin and Galarreta 2005; Dugué et al. 2008). Numerical simulations show that our results are robust to a weak dilution of the connectivity, so that they could apply to these highly coupled local networks. These networks however consist only of tens to hundreds of neurons, and finite-size effects would be prominent (as seen in Fig. 9). To describe faithfully larger networks, the model should take into account a more complex spatial connectivity of the network, where the probability of connection would depend exponentially on the distance between neurons (Dugué et al. 2008). The extension of our

study to such networks with spatial structure is an important direction for future investigations.

Acknowledgements This work was supported by the Agence Nationale de la Recherche grant ANR-05-NEUR-030.

Appendix

A Networks of exponential integrate-and-fire neurons

In order to study the dynamics analytically, we used a model based on leaky integrate-and-fire (LIF) neurons. An important caveat of this approach is that the voltage trace during the action potential is not modeled. To account for electrotonic coupling during the action potential, we assumed that the transmission of the depolarizing part is instantaneous. While this approximation is supported by experimental measurements in fast-spiking cells (Galarreta and Hestrin 2001a), it is important to show that the obtained results, and in particular the bistability between synchrony and asynchrony, are not artifacts of this approximation. In this section, we consider the exponential integrate-and-fire model, which includes a spike-generating sodium current, and thus produces full traces of action potentials. We briefly consider the spikelets produced in this model by the transmission of the action potentials through electrical synapses, and then show that bistability between synchrony and asynchrony is still found in this model.

The exponential integrate-and-fire model is a nonlinear integrate-and-fire model that has been shown to approximate remarkably well the action potential shape, and the dynamic properties of more complex conductance-based models such as the Hodgkin-Huxley model (Fourcaud-Trocmé et al. 2003). The dynamics of the membrane potential of neuron i are given by

$$\tau \frac{\partial V_i}{\partial t} = -V_i + \Delta_T \exp\left(\frac{V_i - V_T}{\Delta_T}\right) + \frac{g_c}{N}\sum_{j\neq i} V_j + \mu_{ext} + \sigma\sqrt{\tau}\eta_i(t) \tag{36}$$

This model includes an exponential spike-generating current: once the membrane potential crosses the threshold V_T, it diverges to infinity in finite time. This divergence represents the firing of an action potential. After the divergence, in the original EIF model, the membrane potential is reset instantaneously to V_r. Since this gives an unrealistic spike shape, we reset the membrane potential to V_r following a linear trajectory during a refractory period τ_{rp}, as was done in Dugué et al. (2008).

One advantage of the EIF model over more complicated models is that it provides a way of modulating the shape of the generated action potential by modifying a single parameter Δ_T. The parameter Δ_T determines the sharpness of spike-initiation: the larger Δ_T, the slower the spike initiation, and the wider the full spike trace. The width of the hyperpolarizing part of the spike can be controlled via the refractory period τ_{rp}. In Fig. 19 we illustrate the effect on a postsynaptic cell of spikes of different width: a wide spike leads to a predominantly excitatory spikelet, while a narrow one elicits a mostly inhibitory spikelet. Note that the shapes of the spikelets are very similar to the ones obtained in the simplified, leaky integrate-and-fire model (cf. Fig. 1).

In Fig. 20, we illustrate the fact that bistability between synchrony and asynchrony is generically found in networks of exponential integrate-and-fire neurons. We display the activity of a network consisting of $N = 50$ neurons. In such a small system, the activity switches spontaneously between the asynchronous and the synchronous state. In this particular example, the firing of neurons in the synchronous state is not as highly coordinated as in the case of LIF neurons displayed in Fig. 9, but the two states can be clearly distinguished.

B Linear stability of the asynchronous state in the homogeneous case

The probability distribution $P(V, t)$ obeys

$$\tau \frac{\partial P(V,t)}{\partial t} = \frac{\partial}{\partial V}\left[(V - \mu_{syn} - \mu_{ext})P(V,t)\right] + \frac{\sigma^2}{2}\frac{\partial^2}{\partial V^2}P(V,t), \tag{37}$$

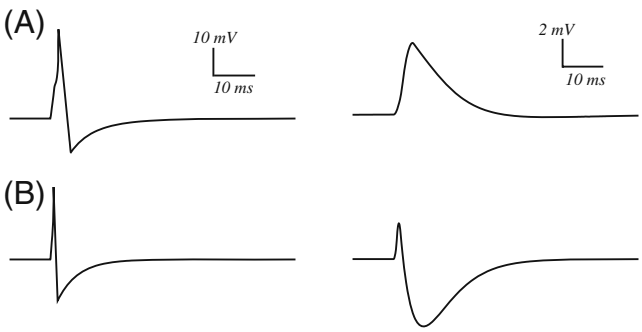

Fig. 19 Spikelets elicited in a post-synaptic cell by the transmission through an electrical synapse of a pre-synaptic spike, obtained from the exponential integrate-and-fire model for two different sets of coupling parameters. (**A**) A wide presynaptic spike leads to a dominantly excitatory spikelet ($V_T = 5.1$ mV, $\Delta_T = 4$ mV, $\tau_{rp} = 3$ ms, $V_r = -10$ mV, holding potential 3 mV); (**B**) a narrow presynaptic spike leads to a dominantly inhibitory spikelet ($V_T = 5.1$ mV, $\Delta_T = 1$ mV, $\tau_{rp} = 1$ ms, $V_r = -10$ mV, holding potential 0 mV)

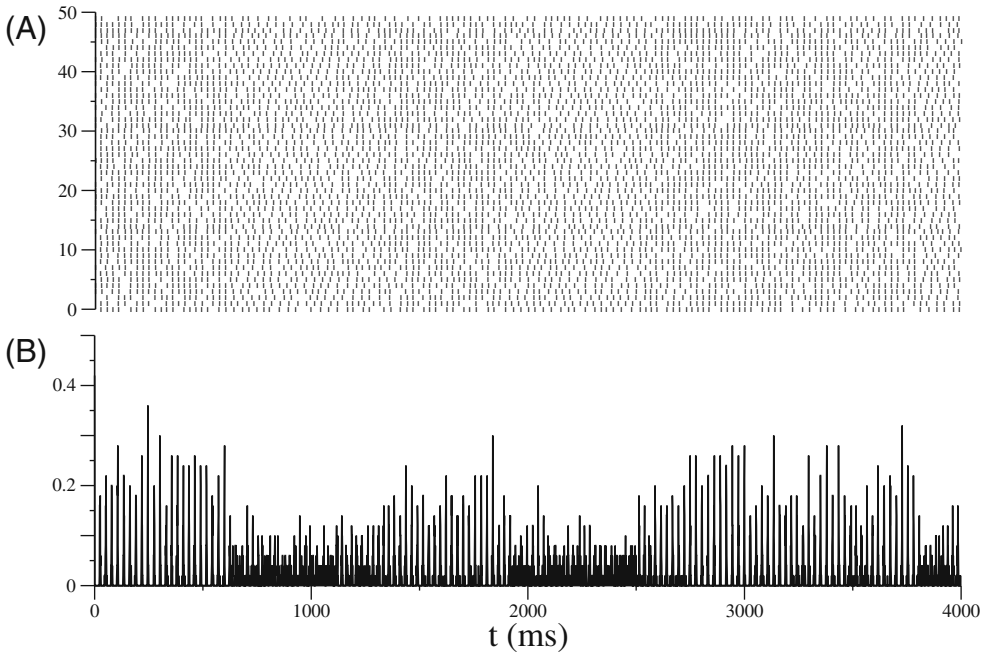

Fig. 20 Bistability in a network of exponential integrate-and-fire neurons: spontaneous transitions between synchrony and asynchrony in a network of $N = 50$ neurons. (**A**) Spike raster of the full network; (**B**) instantaneous population firing rate $\nu(t)$ computed in 1 ms bins. The parameters used in the simulation are: $\mu_{ext} = 3$ mV, $\sigma = 0.47$ mV, $g_c = 0.5$, $V_T = 5.1$ mV, $\Delta_T = 1$ mV, $V_r = -10$ mV, $\tau_{rp} = 1.7$ ms

where $\mu_{syn} = g_c\langle V\rangle + \beta\tau\nu(t)$. The normalization and boundary conditions are:

$$\int_{-\infty}^{V_{th}} P(V,t)dV = 1 \tag{38}$$

$$\int_{-\infty}^{V_{th}} VP(V,t)dV = \langle V(t)\rangle \tag{39}$$

$$\frac{\partial P}{\partial V}(V_{th},t) = -\frac{2\nu(t)\tau}{\sigma^2} \tag{40}$$

$$\frac{\partial P}{\partial V}(V_r^+,t) - \frac{\partial P}{\partial V}(V_r^-,t) = -\frac{2\nu(t)\tau}{\sigma^2}. \tag{41}$$

Multiplying Eq. (37) by V and integrating, we obtain an equation for the evolution of the mean membrane potential $\langle V\rangle$:

$$\tau\frac{d\langle V\rangle}{dt} = (g_c - 1)\langle V\rangle + \mu_{ext} + (\beta - (V_{th} - V_r))\tau\nu(t). \tag{42}$$

From this point on, the analysis follows the same steps as in Brunel and Hakim (1999). We use the rescaled variables $v(t)$, $n(t)$ and $m_{syn}(t)$ defined by:

$$\langle V(t)\rangle = V_0(1 + v(t)), \qquad \nu(t) = \nu_0(1 + n(t)),$$
$$\mu_{syn}(t) = \mu_{syn,0} + m_{syn}(t), \tag{43}$$

$$\mu_{syn,0} = g_c V_0 + \beta\tau\nu_0, \qquad P = \frac{2\tau\nu_0}{\sigma}Q, \tag{44}$$

$$y = \frac{V - \mu_{syn,0} - \mu_{ext}}{\sigma}, \qquad y_{th} = \frac{V_{th} - \mu_{syn,0} - \mu_{ext}}{\sigma},$$
$$y_r = \frac{V_r - \mu_{syn,0} - \mu_{ext}}{\sigma}. \tag{45}$$

With these notations, Eq. (37) becomes

$$\tau\partial_t Q(y,t) = \mathcal{L}[Q] - \frac{m_{syn}}{\sigma}\frac{\partial}{\partial y}Q, \tag{46}$$

where the linear operator $\mathcal{L}$ is defined as

$$\mathcal{L}[Q] = \frac{1}{2}\frac{\partial^2}{\partial y^2}Q + \frac{\partial}{\partial y}(yQ) \tag{47}$$

and the boundary conditions read

$$Q(y_{th},t) = 0, \qquad \frac{\partial Q}{\partial y}(y_{th},t) = -(1 + n(t)) \tag{48}$$

$$[Q]_{y_r^-}^{y_r^+} = 0, \qquad \left[\frac{\partial Q}{\partial y}\right]_{y_r^-}^{y_r^+} = -(1 + n(t)). \tag{49}$$

B.1 Stationary state

The steady-state solution of Eq. (46) is given by

$$Q_0(y) = \begin{cases} \exp(-y^2)\int_y^{y_{th}} du\ \exp(u^2) & y > y_r \\ \exp(-y^2)\int_{y_r}^{y_{th}} du\ \exp(u^2) & y < y_r. \end{cases} \tag{50}$$

The stationary mean membrane potential V_0 is given by Eq. (42):

$$V_0 = \frac{\mu_{ext} + \tau\nu_0(\beta - (V_{th} - V_r))}{1 - g_c}. \tag{51}$$

The stationary firing rate ν_0 is then obtained from the normalization condition Eq. (38):

$$\int_{y_r}^{y_{th}} du\, e^{u^2} \int_{-\infty}^{u} dv e^{-v^2} = \frac{1}{2\tau\nu_0}. \tag{52}$$

As y_r and y_{th} depend on ν_0, Eq. (52) is an implicit equation which can be solved self-consistently for ν_0.

B.2 Linear stability

In the following, we expand the time varying quantities perturbatively at successive orders:

$$\begin{aligned} Q(y,t) &= Q_0(y) + Q_1(y,t) + Q_2(y,t) + \dots \\ n(t) &= n_1(t) + n_2(t) + \dots \\ v(t) &= v_1(t) + v_2(t) + \dots \\ m_{syn}(t) &= m_{syn,1}(t) + m_{syn,2}(t) + \dots \end{aligned} \tag{53}$$

At first order Eq. (46) becomes

$$\tau\partial_t Q_1(y,t) = \mathcal{L}[Q_1] - \frac{m_{syn,1}}{\sigma}\frac{\partial}{\partial y}Q_0. \tag{54}$$

The eigenmodes of Eq. (54) are of the form

$$\begin{aligned} Q_1(y,t) &= \exp\left(\frac{\lambda t}{\tau}\right)\tilde{n}_1(\lambda)\hat{Q}_1(y,\lambda) \\ n_1(t) &= \exp\left(\frac{\lambda t}{\tau}\right)\tilde{n}_1(\lambda) \\ v_1(t) &= \exp\left(\frac{\lambda t}{\tau}\right)\tilde{v}_1(\lambda) \\ m_{syn,1}(t) &= \exp\left(\frac{\lambda t}{\tau}\right)\tilde{m}_1(\lambda) \end{aligned}$$

As $v(t)$ and $n(t)$ are linearly related via Eq. (42)

$$\tilde{v}_1(\lambda) = \frac{\tau\nu_0}{V_0}\frac{\beta - (V_{th} - V_r)}{1 + \lambda - g_c}\tilde{n}_1(\lambda) \tag{55}$$

and

$$\tilde{m}_1(\lambda) = \tau\nu_0 R_g(\lambda)\tilde{n}_1(\lambda) \tag{56}$$

with

$$R_g(\lambda) = \frac{\beta(1+\lambda) - g_c(V_{th} - V_r)}{1 + \lambda - g_c}. \tag{57}$$

$\hat{Q}_1$ therefore obeys the ordinary differential equation

$$\lambda\hat{Q}_1(y,\lambda) = \mathcal{L}[\hat{Q}_1](y,\lambda) - \frac{\tau\nu_0 R_g(\lambda)}{\sigma}\frac{\partial}{\partial y}Q_0, \tag{58}$$

together with the boundary conditions

$$\hat{Q}_1(y_{th},\lambda) = 0, \qquad \frac{\partial\hat{Q}_1}{\partial y}(y_{th},\lambda) = -1, \tag{59}$$

similar conditions at y_r, and the integrability requirement

$$\int_{-\infty}^{y_{th}} dy\,\hat{Q}_1(y,\lambda) < \infty. \tag{60}$$

The general solution of Eq. (58) can be written as

$$\begin{aligned} &\hat{Q}_1(y,\lambda) \\ &= \begin{cases} \alpha_1^+(\lambda)\phi_1(y,\lambda) + \beta_1^+(\lambda)\phi_2(y,\lambda) + \hat{Q}_1^p(y,\lambda) & y > y_r \\ \alpha_1^-(\lambda)\phi_1(y,\lambda) + \beta_1^-(\lambda)\phi_2(y,\lambda) + \hat{Q}_1^p(y,\lambda) & y < y_r \end{cases} \end{aligned} \tag{61}$$

where

$$\hat{Q}_1^p(y,\lambda) = -\frac{1}{1+\lambda}\frac{\tau\nu_0 R_g(\lambda)}{\sigma}\frac{dQ_0(y)}{dy}, \tag{62}$$

and $\phi_{1,2}$ are two independent solutions of the homogeneous equation

$$\frac{1}{2}\phi'' + y\phi' + (1-\lambda)\phi = 0. \tag{63}$$

Solutions of Eq. (63) are obtained in terms of confluent hypergeometric functions (Brunel and Hakim 1999):

$$\phi_1(y,\lambda) = M\left[(1-\lambda)/2, 1/2, -y^2\right] \tag{64}$$

$$\begin{aligned} \phi_2(y,\lambda) = &\frac{\sqrt{\pi}}{\Gamma\left(\frac{1+\lambda}{2}\right)}M\left[(1-\lambda)/2, 1/2, -y^2\right] \\ &+\frac{\sqrt{\pi}}{\Gamma\left(\frac{\lambda}{2}\right)}2yM\left[1-\lambda/2, 3/2, -y^2\right]. \end{aligned} \tag{65}$$

The boundary conditions Eq. (59) give expressions for $\alpha_1^+, \alpha_1^-, \beta_1^+$ and β_1^- as functions of λ:

$$\alpha_1^+ = \tilde{\phi}_2(y_{th},\lambda)\{1 - S_2(y_{th},\lambda)\} \tag{66}$$

$$\beta_1^+ = -\tilde{\phi}_1(y_{th},\lambda)\{1 - S_1(y_{th},\lambda)\} \tag{67}$$

$$\alpha_1^- - \alpha_1^+ = -\tilde{\phi}_2(y_r,\lambda)\{1 - S_2(y_r,\lambda)\} \tag{68}$$

$$\beta_1^- - \beta_1^+ = \tilde{\phi}_1(y_r,\lambda)\{1 - S_2(y_r,\lambda)\}, \tag{69}$$

where

$$\tilde{\phi}_i(y,\lambda) = \frac{\phi_i(y,\lambda)}{Wr[\phi_1,\phi_2](y,\lambda)} \tag{70}$$

$$Wr[\phi_1,\phi_2](y,\lambda) = \phi_1\phi_2' - \phi_2\phi_1' = \frac{\sqrt{\pi}}{\Gamma(\lambda/2)}e^{-y^2} \tag{71}$$

$$S_i(y,\lambda) = \frac{\tau\nu_0}{\sigma}\frac{R_g(\lambda)}{1+\lambda}\left(\frac{\phi_i'}{\phi_i}(y) + 2y\right). \tag{72}$$

The eigenvalues are determined by the requirement (60) that $\hat{Q}_1(y,\lambda)$ be integrable, which corresponds to $\alpha_1^- = 0$, i.e.

$$\left(\tilde{\phi}_2(y_{th},\lambda) - \tilde{\phi}_2(y_r,\lambda)\right) = \tilde{\phi}_2(y_{th},\lambda)S_2(y_{th},\lambda) - \tilde{\phi}_2(y_r,\lambda)S_2(y_r,\lambda) \tag{73}$$

or

$$R_g(\lambda)R_n(\lambda) = 1, \tag{74}$$

with

$$R_g(\lambda) = \frac{(1+\lambda)\beta - g_c(V_{th}-V_r)}{(1-g_c+\lambda)} \tag{75}$$

$$R_n(\lambda) = \frac{\tau\nu_0}{\sigma}\frac{1}{1+\lambda}\frac{\frac{\partial U}{\partial y}(y_{th},\lambda) - \frac{\partial U}{\partial y}(y_r,\lambda)}{U(y_{th}) - U(y_r)} \tag{76}$$

$$U(y,\lambda) = e^{y^2}\phi_2(y,\lambda). \tag{77}$$

B.3 Weakly non-linear analysis

Pushing the development in Eq. (53) to higher orders, it is possible to determine the non-linear contribution to the oscillations in the vicinity of the bifurcation. The n-th order terms obey inhomogeneous linear equations with forcing terms formed by quadratic combinations of lowest-order terms. The dynamics of the first-order oscillation amplitude $\hat{n}_1$ is obtained from a self-consistancy condition on the third order terms, and read

$$\tau\frac{d\hat{n}_1}{dt} = A\hat{n}_1 - B|\hat{n}_1|^2\hat{n}_1 \tag{78}$$

The procedure is identical to the one followed in Brunel and Hakim (1999), we therefore only give here the expressions necessary for evaluating B, and for more details refer the reader to Brunel and Hakim (1999). The results of Brunel and Hakim (1999) are recovered (in the fully connected case $H = 0$) by replacing below $\bar{R}_g(\lambda)$ with $-G_c e^{-\delta\lambda}$.

In the following, we write

$$\bar{R}_g(\lambda) = \frac{\tau\nu_0}{\sigma}R_g(\lambda) \tag{79}$$

$$\tilde{W}_2\left[\hat{Q}\right] = \frac{\hat{Q}\phi_2' - \hat{Q}'\phi_2}{Wr[\phi_1,\phi_2]} \tag{80}$$

B.3.1 Second order The second order terms oscillate at frequencies 0 and $2\omega_c$, and can be written as:

$$Q_2(y,t) = e^{2i\omega_c t/\tau}\hat{n}_1^2\hat{Q}_{2,2}(y) + e^{-2i\omega_c t/\tau}(\hat{n}_1^*)^2\hat{Q}_{2,2}^*(y) + \hat{Q}_{2,0}|\hat{n}_1|^2 \tag{81}$$

$$n_2(t) = e^{2i\omega_c t/\tau}\hat{n}_1^2\rho_{2,2} + e^{-2i\omega_c t/\tau}(\hat{n}_1^*)^2\rho_{2,2}^* + |\hat{n}_1|^2\rho_{2,0}. \tag{82}$$

$\hat{Q}_{2,2}(y)$ can be expressed as

$$\hat{Q}_{2,2}(y) = \begin{cases} \alpha_{2,2}^+\phi_1(y,2i\omega_c) + \beta_{2,2}^+\phi_2(y,2i\omega_c) \\ \quad + \rho_{2,2}\hat{Q}_{2,2}^{so}(y,i\omega_c) + \hat{Q}_{2,2}^{lo} \quad y > y_r \\ \alpha_{2,2}^-\phi_1(y,2i\omega_c) + \beta_{2,2}^-\phi_2(y,2i\omega_c) \\ \quad + \rho_{2,2}\hat{Q}_{2,2}^{so}(y,i\omega_c) + \hat{Q}_{2,2}^{lo} \quad y < y_r, \end{cases} \tag{83}$$

where:

$$\hat{Q}_{2,2}^{so} = -\frac{\bar{R}_g(2i\omega_c)}{1+2i\omega_c}\frac{dQ_0}{dy} \tag{84}$$

$$\hat{Q}_{2,2}^{lo} = \frac{\bar{R}_g(i\omega_c)}{1+i\omega_c}\frac{\partial Q_1}{\partial y} - \frac{\bar{R}_g(i\omega_c)^2}{2(1+i\omega_c)^2}\frac{d^2Q_0}{dy^2} \tag{85}$$

$$\rho_{22} = \frac{\tilde{W}_2\left[\hat{Q}_{2,2}^{lo}\right](y_{th}) - \left[\tilde{W}_2\left[\hat{Q}_{2,2}^{lo}\right](y)\right]_{y_r^-}^{y_r^+}}{(\tilde{\phi}_2(y_{th}) - \tilde{\phi}_2(y_r)) - \tilde{W}_2\left[\hat{Q}_{2,2}^{so}\right](y_{th}) + \left[\tilde{W}_2\left[\hat{Q}_{2,2}^{so}\right](y)\right]_{y_r^-}^{y_r^+}}. \tag{86}$$

Similarly, $\hat{Q}_{2,0}(y)$ can be expressed as

$$\hat{Q}_{2,0}(y) = \begin{cases} \alpha_{2,0}^+Q_0 + \beta_{2,0}^+\exp(-y^2) \\ \quad + \rho_{2,0}\hat{Q}_{2,0}^{so}(y) \quad + \hat{Q}_{2,0}^{lo} \quad y > y_r \\ \alpha_{2,0}^-Q_0 + \beta_{2,0}^-\exp(-y^2) \\ \quad + \rho_{2,0}\hat{Q}_{2,0}^{so}(y,i\omega_c) + \hat{Q}_{2,0}^{lo} \quad y < y_r, \end{cases} \tag{87}$$

where:

$$\hat{Q}_{2,0}^{so} = -\bar{R}_g(0)\frac{dQ_0}{dy} \tag{88}$$

$$\hat{Q}_{2,0}^{lo} = -\left[\frac{\bar{R}_g(-i\omega_c)}{1-i\omega_c}\frac{\partial\hat{Q}_1}{\partial y} + c.c.\right] - \frac{\bar{R}_g(-i\omega_c)\bar{R}_g(i\omega_c)}{(1+\omega_c^2)}\frac{d^2Q_0}{dy^2} \tag{89}$$

$$\rho_{20} = \frac{\left[2\frac{\bar{R}_g(-i\omega_c)}{1+\omega_c^2}(-\bar{R}_g(i\omega_c)y+1)e^{y^2}\int_{-\infty}^{y}du e^{-u^2}\right]_{y_r}^{y_{th}}}{\frac{1}{2\nu_0} - \left[\bar{R}_g(0)e^{y^2}\int_{-\infty}^{y}du e^{-u^2}\right]_{y_r}^{y_{th}}}. \tag{90}$$

B.3.2 Third order The third order terms oscillate at frequencies ω_c and $3\omega_c$:

$$Q_3(y,t) = e^{3i\omega_c t/\tau}\,\hat{Q}_{3,3}(y) + e^{i\omega_c t/\tau}\,\hat{Q}_{3,1}(y) + c.c. \tag{91}$$

$$n_3(t) = e^{3i\omega_c t/\tau}\hat{n}_{3,3}(y) + e^{i\omega_c t/\tau}\hat{n}_{3,1}(y) + c.c. \tag{92}$$

The part $\hat{Q}_{3,1}(y)$ of $Q_3(y,t)$ oscillating at frequency ω_c can be written as

$$\hat{Q}_3(y) = \begin{cases} \alpha_3^+\phi_1(y,i\omega_c) + \beta_3^+\phi_2(y,i\omega_c) + \\ \quad \hat{n}_{3,1}\hat{Q}_1^p(y,i\omega_c) + \hat{Q}_{3,1}^{lo} \quad y > y_r \\ \alpha_3^-\phi_1(y,i\omega_c) + \beta_3^-\phi_2(y,i\omega_c) + \\ \quad \hat{n}_{3,1}\hat{Q}_1^p(y,i\omega_c) + \hat{Q}_{3,1}^{lo} \quad y < y_r, \end{cases} \tag{93}$$

with

$$\hat{Q}_{3,1}^{lo} = \tau\frac{d\hat{n}_1}{dt}\hat{Q}_{3,1}^d + \hat{n}_1\hat{Q}_{3,1}^l + \hat{n}_1|\hat{n}_1|^2\hat{Q}_{3,1}^c, \tag{94}$$

where

$$\hat{Q}_{3,1}^d(y) = \begin{cases} \alpha_1^+\partial_\lambda\phi_1(y,i\omega_c) + \beta_1^+\partial_\lambda\phi_2(y,i\omega_c) + \\ \quad \partial_\lambda\hat{Q}_1^p(y,i\omega_c) \quad y > y_r \\ \beta_1^-\partial_\lambda\phi_2(y,i\omega_c) + \partial_\lambda\hat{Q}_1^p(y,i\omega_c) \\ \quad y < y_r, \end{cases} \tag{95}$$

$$\hat{Q}_{3,1}^l(y) = \frac{\bar{R}_g - \bar{R}_{g,c}}{1+i\omega_c}\frac{dQ_0}{dy}, \tag{96}$$

and

$$\begin{aligned} \hat{Q}_{3,1}^c = &-\frac{\bar{R}_g(-i\omega_c)}{1-i\omega_c}\frac{\partial\hat{Q}_{22}}{\partial y} - \frac{\bar{R}_g(i\omega_c)}{1+i\omega_c}\frac{\partial\hat{Q}_{20}}{\partial y} - \rho_{20}\bar{R}_g(0)\frac{\partial\hat{Q}_1}{\partial y} \\ &-\frac{\rho_{22}\bar{R}_g(2i\omega_c)}{1+2i\omega_c}\frac{\partial\hat{Q}_1^*}{\partial y} - \frac{\bar{R}_g(i\omega_c)^2}{2(1+i\omega_c)^2}\frac{\partial^2\hat{Q}_1^*}{\partial y^2} \\ &-\frac{\bar{R}_g(i\omega_c)\bar{R}_g(-i\omega_c)}{1+\omega_c^2}\frac{\partial^2\hat{Q}_1}{\partial y^2} - \frac{\rho_{20}\bar{R}_g(0)\bar{R}_g(i\omega_c)}{1+i\omega_c}\frac{d^2Q_0}{dy^2} \\ &-\frac{\rho_{22}\bar{R}_g(-i\omega)\bar{R}_g(2i\omega_c)}{(1-i\omega_c)(2i\omega_c+1)}\frac{d^2Q_0}{dy^2} \\ &-\frac{\bar{R}_g(-i\omega)\bar{R}_g(i\omega_c)^2}{2(1-i\omega_c)(i\omega_c+1)^2}\frac{d^3Q_0}{dy^3}. \end{aligned} \tag{97}$$

B.3.3 Final expressions The constants A and B determining the non-linear dynamics of $\hat{n}_1$ read:

$$A = \frac{W_2[\hat{Q}_{3,1}^l](y_{th}) - \left[\tilde{W}_2[\hat{Q}_{3,1}^l](y)\right]_{y_r^-}^{y_r^+}}{W_2[\hat{Q}_{3,1}^d](y_{th}) - \left[\tilde{W}_2[\hat{Q}_{3,1}^d](y)\right]_{y_r^-}^{y_r^+}} \tag{98}$$

$$B = \frac{W_2[\hat{Q}_{3,1}^c](y_{th}) - \left[\tilde{W}_2[\hat{Q}_{3,1}^c](y)\right]_{y_r^-}^{y_r^+}}{W_2[\hat{Q}_{3,1}^d](y_{th}) - \left[\tilde{W}_2[\hat{Q}_{3,1}^d](y)\right]_{y_r^-}^{y_r^+}}, \tag{99}$$

Note that the denominator in these expressions can be rewritten as

$$\begin{aligned} &\tilde{W}_2[\hat{Q}_{31}^d](y_{th}) - \left[\tilde{W}_2[\hat{Q}_{31}^d](y)\right]_{y_r^-}^{y_r^+} \\ &\quad = -(\tilde{\phi}_2(y_{th}) - \tilde{\phi}_2(y_r))\frac{\partial}{\partial\lambda}\bar{R}_g R_n(i\omega_c). \end{aligned} \tag{100}$$

C The heterogeneous case

We consider a distribution of input currents such that neurons in the network receive a mean external current $\mu_{ext} = \bar{\mu}_{ext} + z\,\delta\mu$ with probability $\eta(z)$. Taking into account the interactions, the total current received by a neuron becomes

$$\mu_{tot}(z) = \bar{\mu}_{ext} + z\,\delta\mu + \beta\tau\bar{\nu}(t) + g_c\langle\bar{V}\rangle(t) \tag{101}$$

where $\bar{\nu}$ and $\langle\bar{V}\rangle$ are the mean firing rate and membrane potential in the network, averaged over the heterogeneity. We denote by $\langle\rangle$ the average over neurons with the same z, and by a bar the average over different z.

C.1 Stationary state

In the stationary state, the firing rate of the neuron with total input $\mu_{tot,0}(z) = \bar{\mu}_{ext} + z\,\delta\mu + \beta\tau\bar{\nu}_0 + g_c\bar{V}_0$ is given by

$$\nu_0(z) = \left(2\tau\int_{\frac{V_{th}-\mu_{tot,0}(z)}{\sigma}}^{\frac{V_r-\mu_{tot,0}(z)}{\sigma}} du\, e^{u^2}\int_{-\infty}^{u} dv\, e^{-v^2}\right)^{-1}, \tag{102}$$

where $\mu_{tot,0}(z)$ depends on the stationary average firing rate $\bar{\nu}_0$ and mean membrane potential $\bar{V}_0$, which are unknown at this stage.

Averaging over heterogeneity, we get

$$\bar{\nu}_0 = \int dz\,\eta(z)\nu_0(z) \tag{103}$$

$$\bar{V}_0 = \int dz\ \eta(z) V_0(z)$$
$$= \frac{1}{1-g_c}\left(\bar{\mu}_0 + \beta\tau\bar{\nu}_0 + \tau\bar{\nu}_0(V_r - V_{th})\right). \quad (104)$$

These equations can be solved self-consistently for $\bar{\nu}_0$ and $\bar{V}_0$. The distribution ρ of firing rates in the network is then obtained as

$$\rho(\nu) = \int dz\, \eta(z)\, \delta(\nu - \nu_0(z)) \quad (105)$$

C.2 Linear stability

To determine the linear stability of the asynchronous state, we follow the same steps as in Appendix B. We start by linearizing all the time-dependent quantities around their stationary value:

$$Q(y,z,t) = Q_0(y,z) + Q_1(y,z,t) \quad (106)$$

$$\langle \bar{V} \rangle = V_0(1 + \bar{v}(t)) \quad (107)$$

$$\nu(z) = \nu_0(z)(1 + n(z,t)) \quad (108)$$

$$\bar{\nu} = \bar{\nu}_0(1 + \bar{n}(t)), \quad (109)$$

where $\bar{n}(t) = \frac{1}{\bar{\nu}_0}\int dz\, \eta(z)\nu_0(z)n(z,t)$.

At first order, after expanding Q_1, v, n and $\bar{n}$ in eigenmodes, the Foker-Planck equation becomes

$$\lambda \hat{Q}_1(y,z,\lambda) = \mathcal{L}[\hat{Q}_1] - \frac{\tau\bar{\nu}_0 R_g(\lambda)\bar{n}(\lambda)}{\sigma}\frac{\partial}{\partial y}Q_0 \quad (110)$$

with boundary conditions

$$\hat{Q}_1(y_{th},z,\lambda) = 0, \qquad \frac{\partial \hat{Q}_1}{\partial y}(y_{th},z,\lambda) = -n(z,\lambda) \quad (111)$$

The integrability condition for each z reads:

$$n(z,\lambda) = R_g(\lambda) R_n(\lambda,z)\bar{n}(\lambda) \quad (112)$$

where $R_n(\lambda,z) = \frac{\tau\nu_0(z)}{\sigma}\frac{1}{1+\lambda}\frac{\frac{\partial U}{\partial y}(y_{th},\lambda) - \frac{\partial U}{\partial y}(y_r,\lambda)}{U(y_{th}) - U(y_r)}$

Multiplying both sides of Eq. (112) by $\eta(z)\nu_0(z)$, and integrating over z, we get

$$R_g(i\omega)\bar{R}_n(i\omega) = 1, \quad (113)$$

with

$$\bar{R}_n(i\omega) = \int d\nu \rho(\nu) R_n(i\omega,\nu). \quad (114)$$

D Response to external oscillations

We consider the situation where the external current varies in time as $\mu_{ext}(t) = \mu_{ext,0} + \mu_{ext,1}(t)$, with $\mu_{ext,1}(t) = \tilde{m}_{ext}(\lambda)e^{\lambda t/\tau} + c.c.$, and $\lambda = i\omega$. In that case

$$\tilde{v}_1(\lambda) = \frac{1}{V_0}\frac{\tau\nu_0(\beta - (V_{th} - V_r))\tilde{n}_1(\lambda) + \tilde{m}_{ext}}{1 + \lambda - g_c} \quad (115)$$

so that Eq. (58) becomes

$$\lambda Q_1(y,\lambda) = \mathcal{L}[Q_1](y,\lambda) - \frac{\tau\nu_0 R_g(\lambda) + \frac{1+\lambda}{1+\lambda-g_c}\frac{\tilde{m}_{ext}(\lambda)}{\tilde{n}(\lambda)}}{\sigma}\frac{\partial}{\partial y}Q_0. \quad (116)$$

The condition α_1^- then gives

$$\left(R_g + \frac{1+\lambda}{1+\lambda-g_c}\frac{\tilde{m}_{ext}(\lambda)}{\tau\nu_0\tilde{n}(\lambda)}\right)R_n = 1. \quad (117)$$

Rearranging the terms, we obtain

$$\tau\nu_0\tilde{n}(\lambda) = \frac{1+\lambda}{1+\lambda-g_c}\frac{R_n(\lambda)}{1 - R_n(\lambda)R_g(\lambda)}\tilde{m}_{ext}(\lambda) \quad (118)$$

References

Abbott, L. F., & van Vreeswijk, C. (1993). Asynchronous states in a network of pulse-coupled oscillators. *Physical Review, E, 48*, 1483–1490.

Amit, D., & Brunel, N. (1997). Model of global spontaneous activity and local structured delay activity during delay periods in the cerebral cortex. *Cerebral Cortex, 7*, 237–252.

Beierlein, M., Gibson, J. R., & Connors, B. (2000). A network of electrically coupled interneurons drives synchronized inhibition in neocortex. *Nature Neuroscience, 3*, 904–909

Bem, T., Feuvre, Y. L., Rinzel, J., & Meyrand, P. (2005). Electrical coupling induces bistability of rhythms in networks of inhibitory spiking neurons. *European Journal of Neuroscience, 22*, 2661–2668.

Bennett, M., & Zukin, R. (2004). Electrical coupling and neuronal synchronization in the mammalian brain. *Neuron, 41*, 495–511.

Brunel, N. (2000). Dynamics of sparsely connected networks of excitatory and inhibitory spiking neurons. *Journal of Computational Neuroscience, 8*, 183–208.

Brunel, N., Chance, F., Fourcaud, N., & Abbott, L. (2001). Effects of synaptic noise and filtering on the frequency response of spiking neurons. *Physical Review Letters, 86*, 2186–2189.

Brunel, N., & Hakim, V. (1999). Fast global oscillations in networks of integrate-and-fire neurons with low firing rates. *Neural Computation, 11*, 162–1671.

Brunel, N., & Hakim, V. (2008). Sparsely synchronized neuronal oscillations. *Chaos, 18*, 015113.

Brunel, N., & Hansel, D. (2006). How noise affects the synchronization properties of reccurent networks of inhibitory neurons. *Neural Computation, 18*, 1066–1110.

Chow, C. C., & Kopell, N. (2000). Dynamics of spiking neurons with electrical coupling. *Neural Computation, 12*, 1643–1678.

Connors, B., & Long, M. (2004). Electrical synapses in the mammalian brain. *Annual Review of Neuroscience, 27*, 393–418.

Coombes, S., & Zachariou, M. (2008). Gap junctions and emergent rhythms. In J. Rubin, R. Matias (Ed.), *Coherent behavior in neuronal networks, computational neuroscience series*. New York: Springer.

Coombes, S. (2008). Neuronal networks with gap junctions: A study of piece-wise linear planar neuron models. *SIAM Journal on Applied Dynamical Systems, 7*, 1101–1129.

Draguhn, A., Traub, R., Schmitz, D., & Jefferys, J. (1998). Electrical coupling underlies high-frequency oscillations in the hippocampus *in vitro*. *Nature, 394*, 189–192.

Dugué G., Brunel N., Hakim V., Schwartz E., Chat M., Levesque M., et al. (2008). Electrical coupling mediates tunable low-frequency oscillations and resonance in the cerebellar Golgi network. *Neuron* (in press).

Fourcaud-Trocmé, N., Hansel, D., van Vreeswijk, C., & Brunel, N. (2003). How spike generation mechanisms determine the neuronal response to fluctuating inputs. *Journal of Neuroscience, 23*, 11628–11640.

Fukuda, T., & Kosaka, T. (2000). Gap-junction coupling linking the dendritic network of gabaergic neurons in the hippocampus. *Journal of Neuroscience, 20*, 1519–1528.

Galarreta, M., Erdelyi, F., Szabo, G., & Hestrin, S. (2004). Electrical coupling among irregular-spiking gabaergic interneurons expressing cannabinoid receptors. *Journal of Neuroscience, 24*, 9770–9778.

Galarreta, M., & Hestrin, S. (1999). A network of fast-spiking cells in the neocortex connected by electrical synapses. *Nature, 402*, 72–75.

Galarreta, M., & Hestrin, S. (2001a). Electrical synapses between gaba-releasing interneurons. *Nature Reviews, Neuroscience, 2*, 425–433.

Galarreta, M., & Hestrin, S. (2001b). Spike transmission and synchrony detection in networks of gabaergic interneurons. *Science, 292*, 2295–2299.

Galarreta, M., & Hestrin, S. (2002). Electrical and chemical synapses among parvalbumin fast-spiking gabaergic interneurons in adult mouse neocortex. *Proceedings of the National Academy of Sciences of the United States of America, 00*, 12438–12443.

Gerstner, W., & van Hemmen, J. L. (1993). Coherence and incoherence in a globally coupled ensemble of pulse-emitting units. *Physical Review Letters, 71*, 312–315.

Gibson, J. R., Beierlein, M., & Connors, B. (1999). Two networks of electrically coupled inhibitory neurons in neocortex. *Nature, 402*, 75–79.

Hestrin, S., & Galarreta, M. (2005). Electrical synapses define networks of neocortical gabaergic neurons. *Trends in Neuroscience, 28*, 304–309.

Kopell, N., & Ermentrout, B. (2004). Chemical and electrical synapses perform complementary roles in the synchronization of interneuronal networks. *Proceedings of the National Academy of Sciences of the United States of America, 101*, 15482–15487.

Landisman, C., Long, M., Beierlein, M., Deans, M., Paul, D. & Connors, B. (2002). Electrical synapses in the thalamic reticular nucleus. *Journal of Neuroscience, 22*, 1002–1009.

LeBeau, F., Traub, R., Monyer, H., Whittington, M., & Buhl, E. (2003). The role of electrical signaling via gap junctions in the generation of fast network oscillations. *Brain Research Bulletin, 62*, 3–13.

Lewis, T. J., & Rinzel, J. (2003). Dynamics of spiking neurons connected by both inhibitory and electrical coupling. *Journal of Computational Neuroscience, 14*, 283–309.

Mann-Metzer, P., & Yarom, Y. (1999). Electrotonic coupling interacts with intrinsic properties to generate synchronized activity in cerebellar networks of inhibitory interneurons. *Journal of Neuroscience, 19*, 3298–3306.

Pfeuty, B., Mato, G., Golomb, D., & Hansel, D. (2003). Electrical synapses and synchrony: The role of intrinsic currents. *Journal of Neuroscience, 23*, 6280–6294.

Pfeuty, B., Mato, G., Golomb, D., & Hansel, D. (2005). The combined effects of inhibitory and electrical synapses in synchrony. *Neural Computation, 17*, 633–670.

Risken, H. (1984). *The Fokker Planck equation: methods of solution and applications*. New York: Springer.

Schneider A. R., Lewis T. J., & Rinzel J. (2006). Effects of correlated input and electrical coupling on synchrony in fast-spiking cell networks. *Neurocomputing, 69*, 1125–1129

Sherman, A., & Rinzel, J. (1992). *Proceedings of the National Academy of Sciences of the United States of America, 89*, 2471–2474.

Skinner F. K., Zhang L., Perez Velazquez J.L., & Carlen P. L. (1999). Bursting in Inhibitory Interneuronal Networks: A Role for Gap-Junctional Coupling. *Journal of Neurophysiology, 81*, 1274–1283.

Tamas, G., Buhl, E., Lorincz, A., & Somogyi, P. (2000). Proximally targeted gabaergic synapses and gap junctions synchronize cortical interneurons. *Nature Neuroscience, 3*, 366–371.

Timme, M., Wolf, F., & Geisel, T. (2002). Coexistence of regular and irregular dynamics in complex networks of pulse-coupled oscillators. *Physical Review Letters, 89*, 258701.

Traub, R., Kopell, N., Bibbig, A., Buhl, E., LeBeau, F., & Whittington, M. (2001). Gap junctions between interneuron dendrites can enhance synchrony of gamma oscillations in distributed networks. *Journal of Neuroscience, 21*, 9478–86.

Tuckwell, H. (1988). *Introduction to theoretical neurobiology*. Cambridge: Cambridge University Press.

Venance, L., Rozov, A., Blatow, M., Burnashev, N., Feldmeyer, D., & Monyer, H. (2000). Connexin expression in electrically coupled postnatal rat brain neurons. *Proceedings of the National Academy of Sciences of the United States of America, 97*, 10260–10265.